

**IAEA**

International Atomic Energy Agency

# Nuclear–Concentrated Solar Power Hybrid Energy System Part-Task Simulator

*Manual and Practical Exercises*

NUCLEAR-CONCENTRATED SOLAR  
POWER HYBRID ENERGY SYSTEM  
PART-TASK SIMULATOR

The following States are Members of the International Atomic Energy Agency:

AFGHANISTAN	GAMBIA	OMAN
ALBANIA	GEORGIA	PAKISTAN
ALGERIA	GERMANY	PALAU
ANGOLA	GHANA	PANAMA
ANTIGUA AND BARBUDA	GREECE	PAPUA NEW GUINEA
ARGENTINA	GRENADA	PARAGUAY
ARMENIA	GUATEMALA	PERU
AUSTRALIA	GUYANA	PHILIPPINES
AUSTRIA	HAITI	POLAND
AZERBAIJAN	HOLY SEE	PORTUGAL
BAHAMAS	HONDURAS	QATAR
BAHRAIN	HUNGARY	REPUBLIC OF MOLDOVA
BANGLADESH	ICELAND	ROMANIA
BARBADOS	INDIA	RUSSIAN FEDERATION
BELARUS	INDONESIA	RWANDA
BELGIUM	IRAN, ISLAMIC REPUBLIC OF	SAINT KITTS AND NEVIS
BELIZE	IRAQ	SAINT LUCIA
BENIN	IRELAND	SAINT VINCENT AND THE GRENADINES
BOLIVIA, PLURINATIONAL STATE OF	ISRAEL	SAMOA
BOSNIA AND HERZEGOVINA	ITALY	SAN MARINO
BOTSWANA	JAMAICA	SAUDI ARABIA
BRAZIL	JAPAN	SENEGAL
BRUNEI DARUSSALAM	JORDAN	SERBIA
BULGARIA	KAZAKHSTAN	SEYCHELLES
BURKINA FASO	KENYA	SIERRA LEONE
BURUNDI	KOREA, REPUBLIC OF	SINGAPORE
CABO VERDE	KUWAIT	SLOVAKIA
CAMBODIA	KYRGYZSTAN	SLOVENIA
CAMEROON	LAO PEOPLE'S DEMOCRATIC REPUBLIC	SOUTH AFRICA
CANADA	LATVIA	SPAIN
CENTRAL AFRICAN REPUBLIC	LEBANON	SRI LANKA
CHAD	LESOTHO	SUDAN
CHILE	LIBERIA	SWEDEN
CHINA	LIBYA	SWITZERLAND
COLOMBIA	LIECHTENSTEIN	SYRIAN ARAB REPUBLIC
COMOROS	LITHUANIA	TAJIKISTAN
CONGO	LUXEMBOURG	THAILAND
COSTA RICA	MADAGASCAR	TOGO
CÔTE D'IVOIRE	MALAWI	TONGA
CROATIA	MALAYSIA	TRINIDAD AND TOBAGO
CUBA	MALI	TUNISIA
CYPRUS	MALTA	TÜRKİYE
CZECH REPUBLIC	MARSHALL ISLANDS	TURKMENISTAN
DEMOCRATIC REPUBLIC OF THE CONGO	MAURITANIA	UGANDA
DENMARK	MAURITIUS	UKRAINE
DJIBOUTI	MEXICO	UNITED ARAB EMIRATES
DOMINICA	MONACO	UNITED KINGDOM OF GREAT BRITAIN AND NORTHERN IRELAND
DOMINICAN REPUBLIC	MONGOLIA	UNITED REPUBLIC OF TANZANIA
ECUADOR	MONTENEGRO	UNITED STATES OF AMERICA
EGYPT	MOROCCO	URUGUAY
EL SALVADOR	MOZAMBIQUE	UZBEKISTAN
ERITREA	MYANMAR	VANUATU
ESTONIA	NAMIBIA	VENEZUELA, BOLIVARIAN REPUBLIC OF
ESWATINI	NEPAL	VIET NAM
ETHIOPIA	NETHERLANDS	YEMEN
FIJI	NEW ZEALAND	ZAMBIA
FINLAND	NICARAGUA	ZIMBABWE
FRANCE	NIGER	
GABON	NIGERIA	
	NORTH MACEDONIA	
	NORWAY	

The Agency's Statute was approved on 23 October 1956 by the Conference on the Statute of the IAEA held at United Nations Headquarters, New York; it entered into force on 29 July 1957. The Headquarters of the Agency are situated in Vienna. Its principal objective is "to accelerate and enlarge the contribution of atomic energy to peace, health and prosperity throughout the world".

TRAINING COURSE SERIES No. 81

NUCLEAR–CONCENTRATED SOLAR  
POWER HYBRID ENERGY SYSTEM  
PART-TASK SIMULATOR

MANUAL AND PRACTICAL EXERCISES

INTERNATIONAL ATOMIC ENERGY AGENCY  
VIENNA, 2023

## COPYRIGHT NOTICE

All IAEA scientific and technical publications are protected by the terms of the Universal Copyright Convention as adopted in 1952 (Berne) and as revised in 1972 (Paris). The copyright has since been extended by the World Intellectual Property Organization (Geneva) to include electronic and virtual intellectual property. Permission to use whole or parts of texts contained in IAEA publications in printed or electronic form must be obtained and is usually subject to royalty agreements. Proposals for non-commercial reproductions and translations are welcomed and considered on a case-by-case basis. Enquiries should be addressed to the IAEA Publishing Section at:

Marketing and Sales Unit, Publishing Section  
International Atomic Energy Agency  
Vienna International Centre  
PO Box 100  
1400 Vienna, Austria  
fax: +43 1 26007 22529  
tel.: +43 1 2600 22417  
email: [sales.publications@iaea.org](mailto:sales.publications@iaea.org)  
[www.iaea.org/publications](http://www.iaea.org/publications)

For further information on this publication, please contact:

Nuclear Power Technology Development Section  
International Atomic Energy Agency  
Vienna International Centre  
PO Box 100  
1400 Vienna, Austria  
Email: [Official.Mail@iaea.org](mailto:Official.Mail@iaea.org)

NUCLEAR-CONCENTRATED SOLAR POWER HYBRID ENERGY SYSTEM PART-TASK SIMULATOR:  
MANUAL AND PRACTICAL EXERCISES

IAEA, VIENNA, 2023  
IAEA-TCS-81  
ISSN 1018-5518

© IAEA, 2023

Printed by the IAEA in Austria  
November 2023

## FOREWORD

The IAEA offers its Member States a wide spectrum of education and training activities. These include face-to-face training courses and workshops, on-line learning, fellowship programmes and schools, as well as publications in the IAEA's Training Course Series, including handbooks, textbooks and manuals on various nuclear related topics.

Experience shows that education and training supported by hands-on learning by doing using nuclear power plant simulators is an effective way for a broad range of target groups to meet education and training standards. The IAEA regularly publishes reference material and holds training courses to assist professionals in Member States in understanding nuclear power plant simulators and associated technologies. The education and training courses support an integrated approach that combines lectures with learning by doing on the specifics of plant operation, including reactor physics, thermal hydraulics and safety aspects, using basic principle simulators.

Classification, Selection and Use of Nuclear Power Plant Simulators for Education and Training (IAEA-TECDOC-1887) provides information for educational institutions, training centres and suppliers on the proper classification, selection and use of various types of nuclear power plant simulator. The IAEA also provides opportunities for hands-on learning using nuclear reactor simulation computer programs, either full plant basic principle simulators or part-task simulators addressing specific parts of plant operations (i.e. systems or components) or specific phenomena. The simplified reactor designs of basic principle simulators allow professionals to grasp fundamental concepts without becoming overwhelmed by the details of a more complex, full scope simulator. The objective of these basic principle full plant or part-task simulators is to provide insight into and a practical understanding of the operational characteristics of reactors as well as plant responses to perturbations and accident scenarios. Access to both types of basic principle simulator is available to Member States upon request, and thus represents a valuable resource for teaching and training on a wide range of topics relevant to nuclear power plant design, safety, technology, simulation and operations.

This publication provides a comprehensive explanation of the nuclear-concentrated solar power hybrid energy system part-task simulator as well as practical exercises to help readers become familiar with its use. By engaging in these exercises with the part-task simulator, readers will gain hands-on experience and a deeper understanding of its workings.

The IAEA acknowledges the contributions of the Department of Nuclear Engineering at Pakistan Institute of Engineering and Applied Sciences in the development of the part-task simulator described in this publication.

The IAEA officer responsible for the creation of this publication was T. Jevremovic of the Division of Nuclear Power.

## *EDITORIAL NOTE*

*This publication has been prepared from the original material as submitted by the contributors and has not been edited by the editorial staff of the IAEA. The views expressed remain the responsibility of the contributors and do not necessarily reflect those of the IAEA or the governments of its Member States.*

*Guidance and recommendations provided here in relation to identified good practices represent expert opinion but are not made on the basis of a consensus of all Member States.*

*Neither the IAEA nor its Member States assume any responsibility for consequences which may arise from the use of this publication. This publication does not address questions of responsibility, legal or otherwise, for acts or omissions on the part of any person.*

*The use of particular designations of countries or territories does not imply any judgement by the publisher, the IAEA, as to the legal status of such countries or territories, of their authorities and institutions or of the delimitation of their boundaries.*

*The mention of names of specific companies or products (whether or not indicated as registered) does not imply any intention to infringe proprietary rights, nor should it be construed as an endorsement or recommendation on the part of the IAEA.*

*The authors are responsible for having obtained the necessary permission for the IAEA to reproduce, translate or use material from sources already protected by copyrights.*

*The IAEA has no responsibility for the persistence or accuracy of URLs for external or third party Internet web sites referred to in this publication and does not guarantee that any content on such web sites is, or will remain, accurate or appropriate.*

## CONTENTS

1.	INTRODUCTION .....	1
1.1.	BACKGROUND .....	1
1.2.	OBJECTIVE .....	2
1.3.	SCOPE.....	2
1.4.	STRUCTURE .....	2
2.	HYBRID ENERGY SYSTEMS.....	2
2.1.	HISTORICAL BACKGROUND .....	2
2.2.	PROMINENT CHARACTERISTICS OF NUCLEAR-SOLAR HYBRID ENERGY SYSTEM WITHIN THE PART-TASK SIMULATOR .....	4
2.2.1.	Concentrated solar power plant .....	5
2.2.2.	Rankine cycle.....	8
2.3.	LIMITATIONS AND ASSUMPTIONS .....	9
3.	GENERAL INSTRUCTIONS .....	9
3.1.	INSTALLATION .....	9
3.2.	START UP .....	9
3.3.	MODES .....	11
3.3.1.	Global plots mode.....	11
3.3.2.	Simulator mode.....	13
4.	EXAMPLES .....	14
4.1.	MONTHLY POWER VARIATION (GLOBAL PLOTS MODE) .....	14
4.1.1.	Simulation steps.....	15
4.1.2.	Analysis of the output parameters .....	15
4.2.	HOURLY POWER VARIATION (SIMULATOR MODE).....	19
4.2.1.	Simulation steps.....	19
4.2.2.	Analysis of the output parameters .....	21
4.3.	EFFECT OF LATITUDE ON OUTPUT PARAMETERS (GLOBAL PLOTS MODE).....	22
4.3.1.	Simulation steps.....	22
4.3.2.	Analysis of the output parameters .....	22
4.4.	EFFECT OF CORE OUTLET TEMPERATURE ON CYCLE MASS FLOW AND EFFICIENCY (GLOBAL PLOTS MODE) .....	25
4.4.1.	Simulation steps.....	25
4.4.2.	Analysis of the output parameters .....	26
4.5.	EFFECT OF LONGITUDE AND TIME ZONE ON DIRECT NORMAL IRRADIANCE (GLOBAL PLOTS MODE).....	27
4.5.1.	Simulation steps.....	28
4.5.2.	Analysis of output parameters .....	28
	REFERENCES.....	31
	ANNEX I .....	33
	ANNEX II .....	39
	ABBREVIATIONS.....	45
	CONTRIBUTORS TO DRAFTING AND REVIEW .....	47





# 1. INTRODUCTION

## 1.1. BACKGROUND

In support of human resource development in Member States, the IAEA has established education and training programmes on active learning about nuclear technologies using basic principle nuclear power plant and part-task simulators. As part of this programme, the IAEA arranges for the development and distribution of its suites of basic principle simulators including the manuals and related documentation, supports education and training courses and workshops on physics and technology of advanced reactors, methodology on technology assessment and technology relevant databases.

Hands-on learning using nuclear power plant simulators has become an essential tool for education and training programmes worldwide. Experience shows that simulators are effective in allowing a broad range of target groups to meet education and training standards. The International Atomic Energy Agency (IAEA) has been at the forefront of promoting and supporting the use of simulators for education and training purposes. The IAEA TECDOC-1887 on Classification, Selection and Use of Nuclear Power Plant Simulators for Education and Training provides guidance for educational institutions, training centres, and suppliers on the proper classification, selection, and use of various types of simulators [1]. The IAEA assists Member States by providing education and training courses on the physics and technology of nuclear power plant operation through hands-on learning with nuclear reactor simulation computer programs. The programs may refer to full plant basic principle simulators or to part-task simulators addressing specific parts of plant operations (systems or components) or specific phenomena. Both types of basic principle simulators are available to Member States upon request, representing an accessible resource for teaching and training on a wide range of topics relevant to nuclear power plant design, safety, technology, simulation, and operations. The basic principle simulators available through the IAEA often feature simplified reactor designs, allowing professionals to grasp fundamental concepts without becoming overwhelmed by the details of a more complex, full-scope simulator. The objective of these simulators is to provide insight into and a practical understanding of reactor operational characteristics and plant responses to transient and accident scenarios. This type of learning is critical for nuclear power plant personnel, who must be trained to respond quickly and appropriately in transient and accidental conditions. The IAEA regularly publishes reference material and holds education and training courses to assist professionals in Member States in understanding simulators and associated technologies. Education and training courses support an integrated approach that combines lectures with learning by doing on the specifics of plant operation, including reactor physics, thermal hydraulics, and safety aspects, using basic principle simulators.

This publication provides description relevant to understanding basic principles of hybrid energy systems (HES) configuration and working, in which nuclear power plant and renewable energy source are coupled to work in synergy to produce desirable outputs. Detailed description

of nuclear-concentrated solar power (CSP) HES part-tasks simulator is provided together with the exercises applicable to education and training courses and workshops, or self-learning.

## 1.2. OBJECTIVE

The objectives of this publication are to:

- Serve as a reference for lectures on basic principles of HES configuration and operation;
- Support Member States intending to use IAEA part-tasks simulators in national education and training programmes with a resource for necessary background information on theory of HES operation;
- Serve as a reference for students and trainees, who may be unfamiliar with reactor operation in synergy with renewable energy source (e.g., engineering safety, physical sciences, non-nuclear engineering fields, and including non-technical fields) to understand the integration of nuclear and renewables at a basic level;
- Provide exercises for use in education and training courses, use by Member State institutions, or direct use by students or trainees.

## 1.3. SCOPE

The scope of this publication is to explain the underlying phenomena, modelling methodology, and application of nuclear-solar HES. Explanations and examples are limited to light water reactors. Other similar publications address different types of nuclear-renewable HES. Following an overview of HES configuration and operation, this publication provides explanations about the part-task simulator and examples to study.

## 1.4. STRUCTURE

This publication contains the following descriptions:

- **Hybrid energy systems (Section 2)** which provides general purpose overview and designs, such as the basic configuration and function of systems and components, relevant to later explanations;
- **General Instructions (Section 3)** regarding nuclear-CSP part-task simulator including its configuration, modelled systems, and installation;
- **Examples (Section 4)** containing practical exercise of various HES analysis and functions, with explanations about parameter trends and values.

# 2. HYBRID ENERGY SYSTEMS

## 2.1. HISTORICAL BACKGROUND

Global energy demand is increasing driven by increasing population, comfort standards and rapid industrialization. World energy demand is estimated to increase by 34% at the year 2035 [2]. Energy needs are mostly met using conventional energy sources, though other energy

sources also emerged. Traditional energy sources add large proportion of CO<sub>2</sub> emissions to the environment and are chief contributor to global warming. Carbon emissions rose from 21 Gt CO<sub>2</sub> in 1990 to 34 Gt CO<sub>2</sub> in 2019 [3]. Alternative energy sources have, therefore, emerging popularity. Such options include nuclear and renewables.

Nuclear energy is high energy density, green and proven technology that is widely employed across the globe. Besides, nuclear power plants (NPPs) are baseload plants, and have high amount of capital costs when compared to renewable energy sources. NPPs have lower carbon footprint as compared to renewable energy sources for the same amount of energy [4]. Many NPPs are designed to load-follow and are originally outfitted with automatic grid control features [5]. In the meantime, modern NPPs are designed to have strong manoeuvring capabilities unlike some old power units [6]. Small modular reactors (SMRs) are advanced nuclear reactor designs that have a power capacity of up to 300 MWe per unit, which is about one-third of the generating capacity of traditional large water cooled NPPs [7]. Several SMR units can be employed to provide flexible power output. Their short refuelling periods, less capital investment, safety systems and more flexibility make them feasible to be employed in remote areas and towns where load demand is not flat [7]. Currently there are over 80 SMR designs [8].

Fossil fuel based energy sources especially coal, are a major contributor in world's energy blend. About 80% of total global energy supply is affiliated with conventional energy sources based on fossil fuel by the end of 2019 [9]. However, these traditional energy sources are responsible for global warming, pollution, and greenhouse gas emissions. Renewable energy sources include solar energy, hydro, wind, geothermal, and tidal energy [10].

Solar energy is uniformly distributed energy source which is freely available and sustainable. It is believed to be the green and passive energy source. There are many configurations for harnessing the solar power. Major types include photovoltaic cells, and CSP. Both types have their own pros and cons [11]. In CSP plant, sunlight is concentrated on an absorber material by making use of reflecting surfaces where the energy from sunlight is stored in a working fluid (molten salt, liquid sodium, and water) as thermal energy. The thermal energy from the working fluid is then used either for in Rankine cycle or in process heat applications like desalination, district heating, hydrogen production, or steam methane reforming.

The concept of integrating two or more energy sources to form a cooperatively controlled multisource system providing responsive generation to the power grid is referred to as hybrid energy systems (HES) [12]. Nuclear-renewable HES consider opportunities to couple these energy generation sources to leverage the benefits of each technology to provide reliable, sustainable, and flexible electricity to the grid and to provide low carbon energy to other energy use sectors as discussed in the IAEA Nuclear Energy Series on Nuclear-Renewable Hybrid Energy Systems [13]. Nuclear-renewable HESs can produce heat, electricity, and other products that society requires while supporting higher penetrations of variable renewable generation. Such systems therefore can provide energy to support various applications, such as seawater or brackish water desalination, hydrogen production, district heating or cooling, the

extraction of tertiary oil resources, and process heat applications such as cogeneration, coal-to-liquid conversion, and assistance in the synthesis of chemical feedstock [12]. By connecting renewable power plant with a nuclear power plant, the plant can be operated in both static and dynamic load conditions. Nuclear power plants serve as base load providers. Renewable serves to provide fluctuating power output because of their hourly and seasonal intermittency. Various researchers presented the ideas for thermodynamic coupling of nuclear energy with solar energy. These include superheating and reheating in Rankine cycle with solar thermal energy [14], distributed power sourcing [15], and exergy calculations of hybrid energy system using phase change material storage [16].

## 2.2. PROMINENT CHARACTERISTICS OF NUCLEAR-SOLAR HYBRID ENERGY SYSTEM WITHIN THE PART-TASK SIMULATOR

The nuclear-solar HES provides thermodynamic coupling between Rankine cycle and a CSP plant. Rankine cycle power plant is mainly operated using thermal energy of attached SMR. CSP plant provides the assistance to Rankine cycle power plant. Thermal energy obtained from heliostat field of CSP plant is used in Rankine cycle for preheating the feedwater before it enters steam generator of the SMR. This preheating allows feedwater to reach a state close to the saturated liquid by consuming most of sensible heat in the preheater. Since, more heat is now added into the Rankine cycle (SMR and CSP plant), there are two choices to cater this additional energy. The first one is to allow the steam exiting from steam generators to reach more degree of superheat, whereas the second one is to inject more liquid mass per second into the system to restrict turbine inlet temperature at design point. In former choice, turbine observes temperature fluctuations at its inlet which causes thermal shocks and thermal fatigue on the turbine blades and casing. While, in latter choice, mass flow rate of the Rankine cycle seems to vary according to heat addition in the Rankine cycle, which can cause inertial fatigue on plant components. In general, power plant is also associated with leakage of feedwater from its components and a makeup water system is always there to cater its needs. Thus, variation of feedwater mass flow rate in a power plant is not new and can easily be dealt with. Therefore, the second choice seems more reasonable, safe, and easier to handle. Varying amount of steam entering the turbine produces varying power output. This fluctuating output power can be efficiently utilized for areas where power demand curve is wavy.

FIG. 1 shows nuclear-solar HES schematics<sup>1</sup>. It consists of Rankine cycle integrated with CSP plant. Subcooled water is initially pumped to high pressure (stream 1 → 2) and sent to a preheater which is thermally coupled with CSP plant. Thermal energy accumulated in CSP receiver provides major portion of sensible heat to the feedwater coming from pump and increases the feedwater temperature near to saturated temperature (stream 2 → 3). This feedwater leaves the preheater and flows into steam generator (stream 3 → 4) to be converted into superheated steam. Superheated steam expands in the turbine thereby rotating its blades to produce power. The two-phase (liquid-vapour) mixture of water leaves the turbine (stream 4 → 5). This mixture then gives off its latent heat in the condenser (stream 5 → 1) and subcooled

---

<sup>1</sup> SMRs have built-in steam generators

liquid leaves the condenser which is then pumped again into the feedwater-preheater (stream 1 → 2) to complete the cycle. The underlying principle behind thermodynamic coupling of SMR and CSP plant, is that the thermal energy produced in CSP plant is utilized in the preheating section of Rankine cycle (i.e., preheating of feedwater is performed by solar energy instead of turbine bleeds). This method injects more heat into the Rankine cycle due to which power conversion in turbine is increased. Thermal energy obtained from CSP plant is intermittent; it varies hourly and daily because of rotation of earth around its own axis and around the Sun. By varying the amount of preheating to feedwater, the mass flow rate flowing through Rankine cycle varies which results in fluctuating power output. The variable power output can be beneficial for sites which possess wavy load demand. However, the base load is always provided by the SMR irrespective of the power output from the CSP plant.

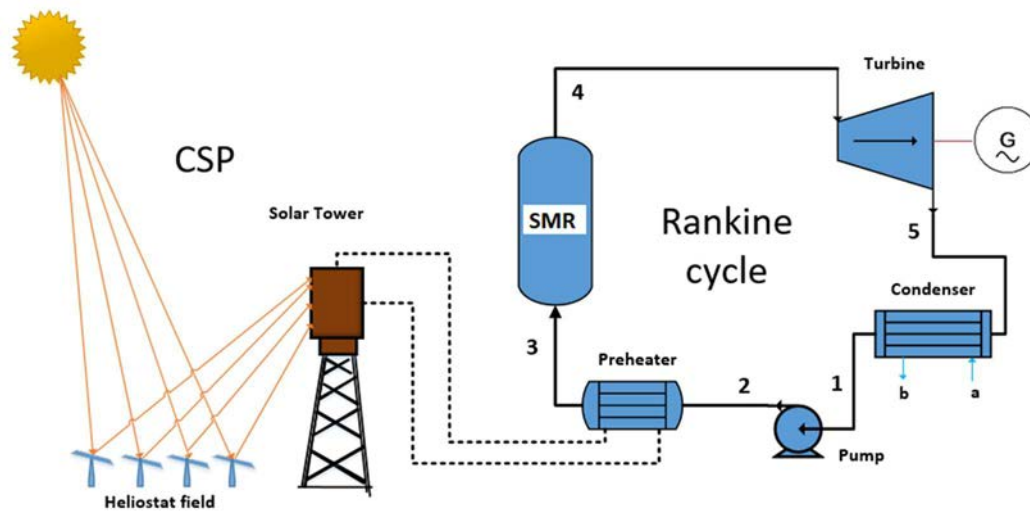


FIG. 1. Configuration and layout of the nuclear-solar HES.

### 2.2.1. Concentrated solar power plant

There are various configurations of CSP plant technologies. They include:

- Line focusing: parabolic trough and linear fresnel;
- Point focusing: parabolic dish and solar power tower

Each of these technologies has its pros and cons, and can be employed considering various factors including site feasibility, solar potential, capital availability, and technology readiness level. CSP plant within the HES part-task simulator uses solar power tower located centrally in a large heliostat field. The heliostat fields may have multiple spatial arrangement. The solar power tower acts as a receiver that collects energy from sunlight reflected from heliostats. It contains a heat transfer medium/working fluid that stores the heat as a thermal energy. In this way, solar thermal energy is concentrated or accumulated in the receiver. This stored thermal energy is then transferred to Rankine cycle for preheating the feedwater, via a series of pumps and heat exchangers. Governing equations for solar power tower of CSP plant are found in [17].

To perform calculations for heliostat field, position of Sun must be known. Sun position is given by solar altitude angle  $\alpha_s$  and solar azimuth angle  $A_s$  which are determined as follows [18]:

$$\alpha_s = \sin(\cos \varphi \cdot \cos \delta \cdot \cos \omega + \sin \varphi \cdot \sin \delta) \quad (1)$$

$$A_s = \arccos\left(\frac{(\sin \varphi \cdot \sin \alpha_s - \sin \delta)}{\cos \alpha_s \cdot \cos \varphi}\right) \quad (2)$$

where:

$\omega$ : solar hour angle

$\varphi$ : local altitude

$\delta$ : declination angle.

The solar hour angle  $\omega$  and declination  $\delta$  are given by:

$$\omega = 15\pi(\tau - 12)/180 \quad (3)$$

$$\delta = 23.45 \cdot \pi \cdot \frac{\sin\left(\frac{2\pi(284+n)}{365}\right)}{180} \quad (4)$$

where  $n$  is ordinal date starting at 1<sup>st</sup> January and  $\tau$  is solar time. Optical efficiency of heliostat field is calculated from HFLCAL (Heliostats Field Layout Calculations) model [19], [20]. Sunlight flux reflected on to the receiver by each mirror (heliostat) is approximated to form a circular Gaussian distribution given by:

$$F(x, y) = DNI \cdot \rho_{hel} \cdot \cos w \cdot f_{atm} \cdot f_{s\&b} \cdot f_{ref}(x, y) \quad (5)$$

where,  $f_{ref}(x, y)$  is the interception efficiency loss,  $w$  is the angle between incident ray and the normal to heliostat surface,  $f_{s\&b}$  is the shadowing and blocking factor associated with neighboring heliostats calculated by MCRT method [21]–[23][22],  $\rho_{hel}$  is the reflectivity and cleanness efficiency,  $DNI$  is direct normal irradiance, and  $f_{atm}$  is the atmospheric attenuation factor. The interception efficiency loss is reflected energy from the heliostats that does not fall onto the receiver, and it depends on both, the heliostat field and the absorber design. It can be written as follows:

$$f_{ref}(x, y) = \frac{\exp\left(-\frac{(x-x_a)^2+(y-y_a)^2}{2\sigma_{tot}^2}\right)}{2\pi\sigma_{tot}^2} \quad (6)$$

where  $(x_a, y_a)$  is the center of cavity aperture, and  $\sigma_{tot}$  is the dispersion of Gaussian distribution which accounts for Sun shape. Gaussian dispersion factor can be determined as follows:

$$\sigma_{tot} = \frac{\sqrt{a^2 \cdot (\sigma_{sun}^2 + 4\sigma_{slo}^2 + \sigma_{ast}^2 + \sigma_{tra}^2)}}{\cos rec} \quad (7)$$

where:

$rec$ : angle between reflected ray and normal to cavity aperture.

$\sigma_{sun}$ ,  $\sigma_{slo}$ ,  $\sigma_{tra}$ : provided in TABLE 1;

$\sigma_{ast}$ : determined as follows:

$$\sigma_{ast} = \frac{\sqrt{W_h \cdot L_h \left[ \frac{1}{\left(\frac{d}{f_{hel}} - \cos w\right)^2} + \frac{1}{\left(d \frac{\cos w}{f_{hel}} - 1\right)^2} \right]}}{4 \cdot d} \quad (8)$$

where:

$W_h$ : width of the mirror;

$L_h$ : length of the mirror

$d$ : distance between heliostat and the receiver;

$f_{hel}$ : focal distance of the heliostat surface.

TABLE 1. NUCLEAR-SOLAR HES PARAMETERS

Parameter	Value
Ambient pressure ( $P_o$ )	101 325 Pa
Ambient temperature ( $T_o$ )	25 °C
Rankine cycle Turbine inlet temperature ( $T_4$ )	$T_{co,SMR} - 10$
Rankine cycle condenser pressure ( $P_1$ )	6.9 kPa
Rankine cycle boiler pressure ( $P_2$ )	6.9 MPa
Steam generator pinch point temperature difference ( $\Delta T_{pp,SG}$ )	10 °C
Turbine isentropic efficiency ( $\eta_{turb}$ )	1.0
Pump isentropic efficiency ( $\eta_{pum}$ )	1.0
Cavity aperture length ( $L_{ape}$ )	12 m
Cavity aperture width ( $W_{ape}$ )	12 m
Number of effective mirrors ( $N_h$ )	1856
Mirror length ( $L_h$ )	12 m
Mirror width ( $W_h$ )	12 m
Reflectivity factor	0.9
Cleanness factor	0.97
Effective tower height ( $H_t$ )	120 m
Tracking error deviation ( $\sigma_{tra}$ )	0.1 mrad
Slope error deviation ( $\sigma_{slo}$ )	0.1 mrad
Sun shape error deviation ( $\sigma_{sol}$ )	9.3 mrad
Interception efficiency	0.95

To reduce the calculation time, a constant value of 0.95 is assumed for the interception efficiency [24]. The  $DNI$  can be calculated as follows, [23]:

$$DNI = \left[ 1367 \cdot \left[ 1 + 0.033 \cdot \cos \left( \frac{2n\pi}{365} \right) \right] \cdot \frac{\sin \alpha_s}{\sin \alpha_s + 0.33} \right] \quad (9)$$

Atmospheric attenuation factor can be calculated by:

$$f_{atm} = \{0.99321 - 0.00176 \cdot d + 1.97 \times 10^{-8} \cdot d^2, \quad d \leq 1000m \quad (10)$$

$$f_{atm} = \exp(-0.0001106 \cdot d), \quad d \geq 1000m \quad (11)$$



$$\cos w = \frac{\sqrt{2}}{2} \cdot [\sin \alpha_s \cdot \cos \lambda - \cos \alpha_s \cdot \sin \lambda \cdot \cos(\theta_h - A_s) + 1]^{0.5} \quad (12)$$

where  $\theta_h$  is the azimuth angle of a given heliostat and  $\lambda$  is an angle between gravity direction and straight line connecting the heliostat and the receiver. Finally, optical efficiency of heliostat field is defined as:

$$\eta_{hel} = \frac{Q_{hel,out}}{Q_{hel,in}} = \frac{\sum_{i=1}^{N_h} \iint F(x,y) dx dy}{\sum_{i=1}^{N_h} DNI \cdot L_h \cdot W_h} \quad (13)$$

FIG. 2 shows distribution of heliostat field of the CSP plant utilized in the HES.

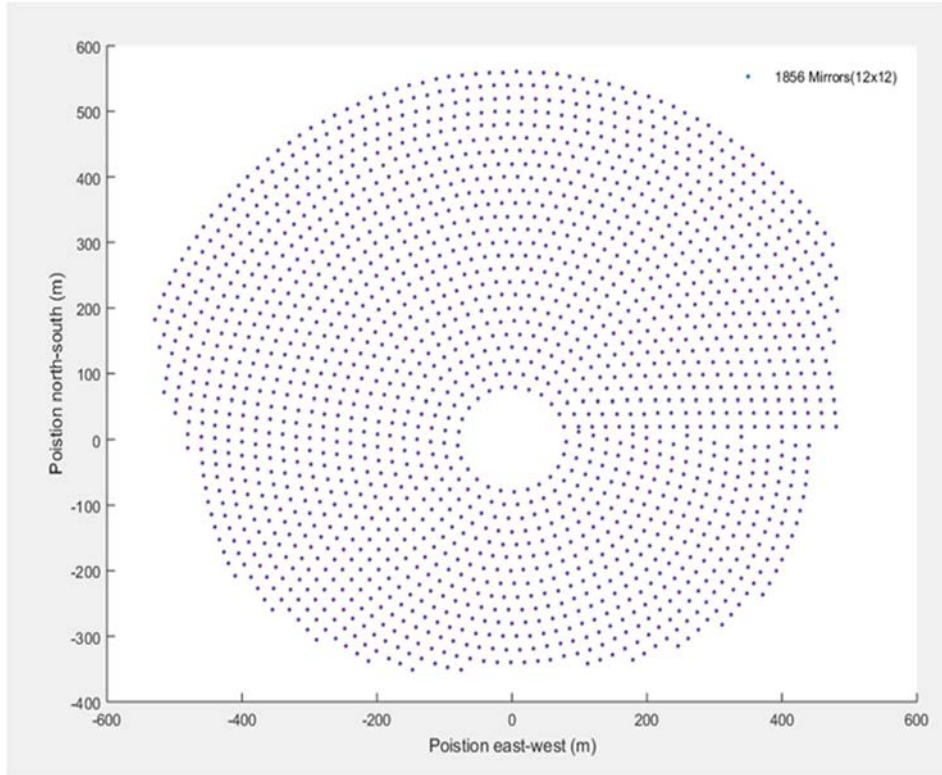


FIG. 2. Heliostat field of the CSP plant.

### 2.2.2. Rankine cycle

Basic Rankine cycle consists of four major components: steam generator, turbine, condenser, and pump. Governing equations for each of the component are provided as follows:

— Heat balance across steam generator (Rankine side) is expressed with:

$$Q_{sg} = \sum m h_{out} - \sum m h_{in} \quad (14)$$

where  $m$  is the cycle mass flow rate.

— Condenser heat duty ( $Q_{cond}$ ) can be found using following heat balance expression:

$$Q_{cond} = \sum mh_{in} - \sum mh_{out} \quad (15)$$

- Turbine power can be calculated using enthalpy balance of streams entering and exiting the turbine:

$$W_t = m \cdot (h_{in} - h_{out}) \quad (16)$$

- Pumping power can be obtained from:

$$W_p = m \cdot v_{f1} \cdot (P_2 - P_1) = m \cdot (h_{out} - h_{in}) \quad (17)$$

where,  $P_1$  and  $P_2$  are condenser and boiler pressure, respectively.

### 2.3. LIMITATIONS AND ASSUMPTIONS

The nuclear-solar HES part-task simulator observes the following limitations and assumptions:

- Ambient pressure and temperature are 1.01 MPa and 25°C, respectively;
- In Rankine cycle, the boiler and condenser pressure are kept at 6.9 MPa and 6.9 kPa, respectively;
- Frictional pressure loss is neglected in all subsystems;
- Heat losses from system components to surroundings are assumed to be negligible;
- Net thermal energy accumulated at the receiver of the CSP plant is assumed to be entirely consumed by a preheater of the Rankine cycle;
- All heat exchangers involved in the system are designed based on the approach temperature model.

## 3. GENERAL INSTRUCTIONS

### 3.1. INSTALLATION

The simulator software is available as an executable installer. The installer will install the application needed to enable user to run the nuclear-solar HES part-task simulator. A zipped file with “.rar” extension is provided to the user which can be extracted to any folder.

### 3.2. START UP

Once the part-task simulator is installed, follow these steps:

- After the extraction is complete, the folder must contain an “.exe” file named “CSP.exe”;
- Opening this file will run the simulator and the home page will appear as shown in FIG. 3;
- Click “Start” button (highlighted in FIG. 3) at the bottom of the window to begin using the simulator;

- A window shown in FIG. 4 will appear with required total of seven input fields. First three inputs are related to the specifications of NPP listed under “NPP Specifications”. The NPP is to be utilized as a base load source in HES, which will usually be an SMR, though another large nuclear reactor can also be used. The other two inputs under “Solar Specifications” are for the coordinates and time zone of the HES site. These coordinates are used for finding parameters of CSP plant;
- After entering the required inputs, click the “Calculate” button (FIG. 4) which solves the thermodynamic model of HES.

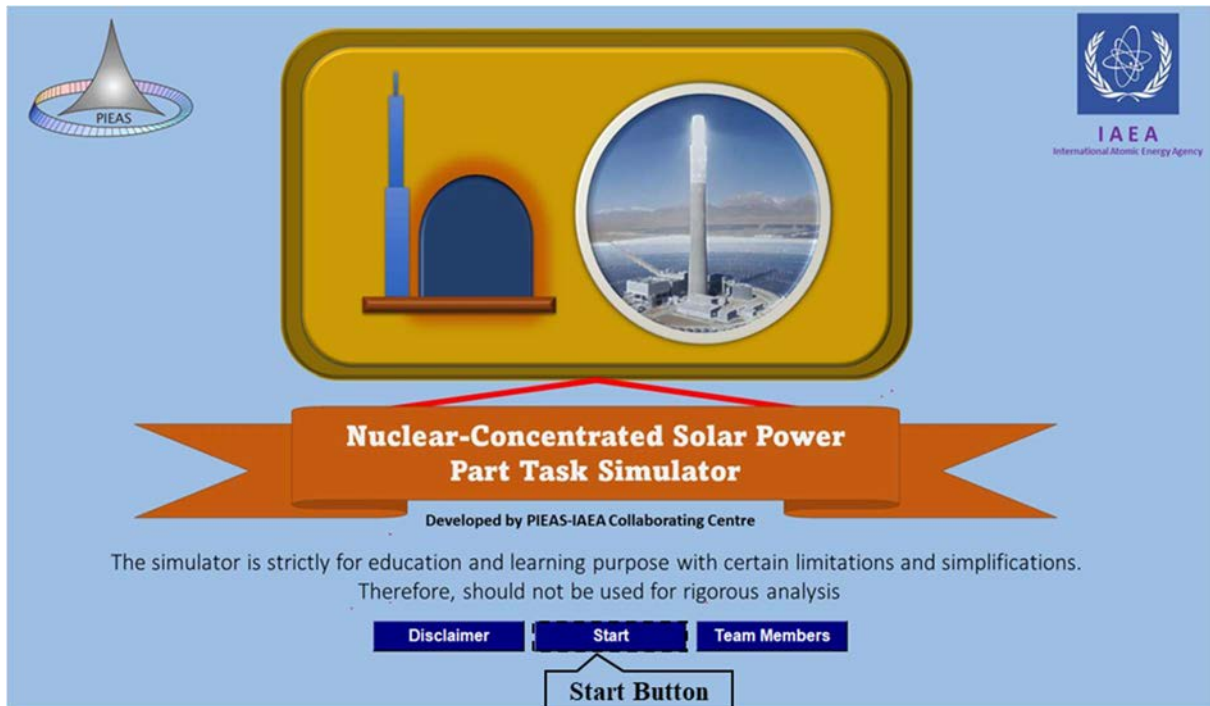


FIG. 3. Nuclear-solar HES part-task simulator: home page.

NPP Specifications	
NPP Thermal Power (MWth)	575
Core Outlet Temperature (C)	320
Number of Modules	2

Solar Specifications	
Latitude (Degrees)	30
Longitude (Degrees)	67
Time Zone (GMT)	+5

**Calculate**

FIG. 4. Nuclear-solar HES part-task simulator: input parameters.

### 3.3. MODES

Nuclear-solar HES part-task simulator provides two modes: *global plots* mode and *simulator* mode under the “Output panel” as shown in FIG. 5. Descriptions of these modes are provided in the following sections.

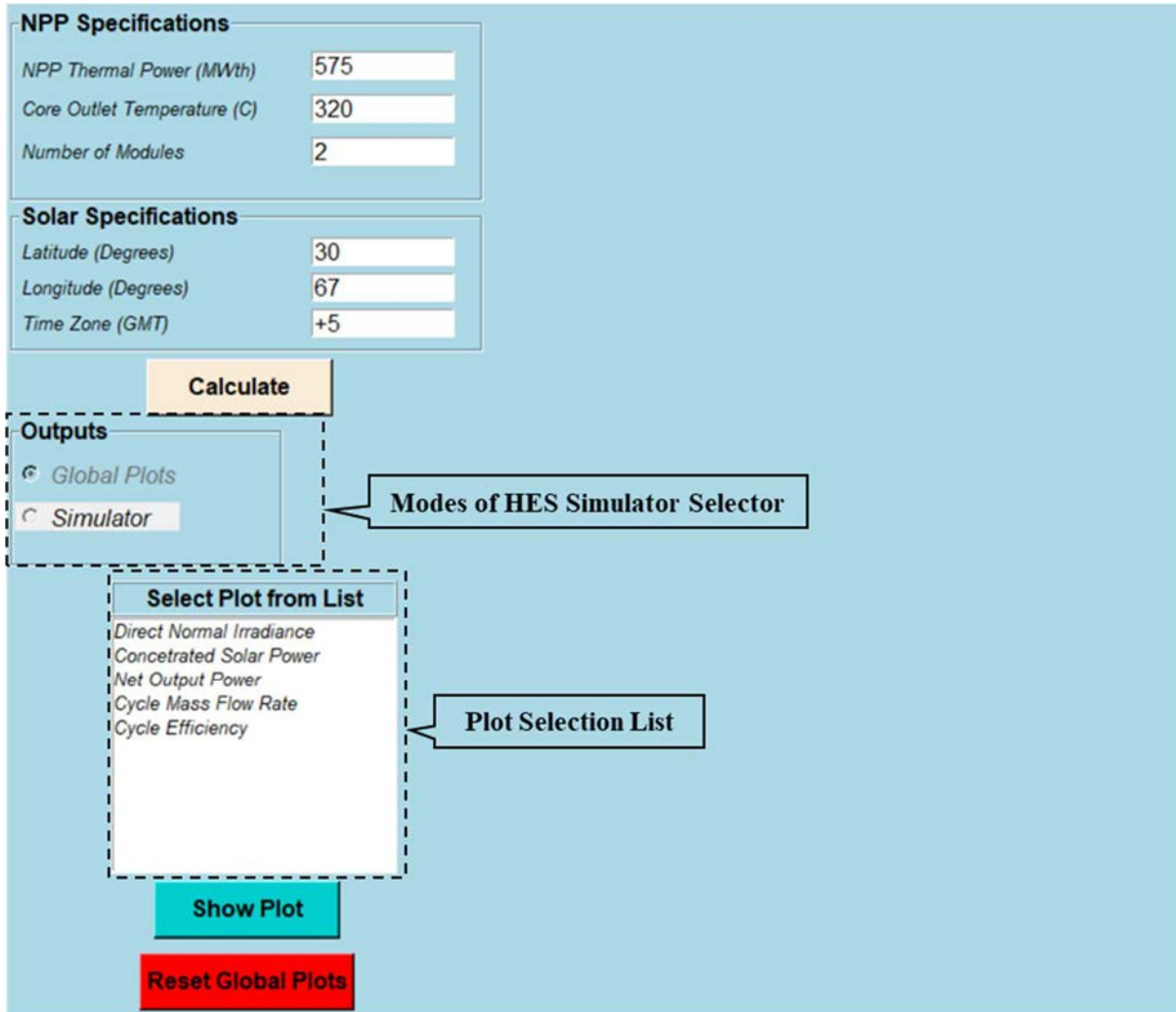


FIG. 5. Nuclear-solar HES part-task simulator: global plots mode and simulator mode.

#### 3.3.1. Global plots mode

“Global Plots” mode provides graphical interpretation of the HES major parameters which includes:

- *DNI*;
- Concentrated power;
- Net electric output power;
- Cycle mass flow rate;
- Cycle efficiency.

Clicking on any one of these parameters and pressing “Show Plot” displays yearly trend of that parameter, as shown in FIG. 5 and FIG. 6. The  $x$  axis in FIG. 6 represents 12 months in a year and  $y$  axis represents quantity for which yearly variation is displayed (selected from the list).

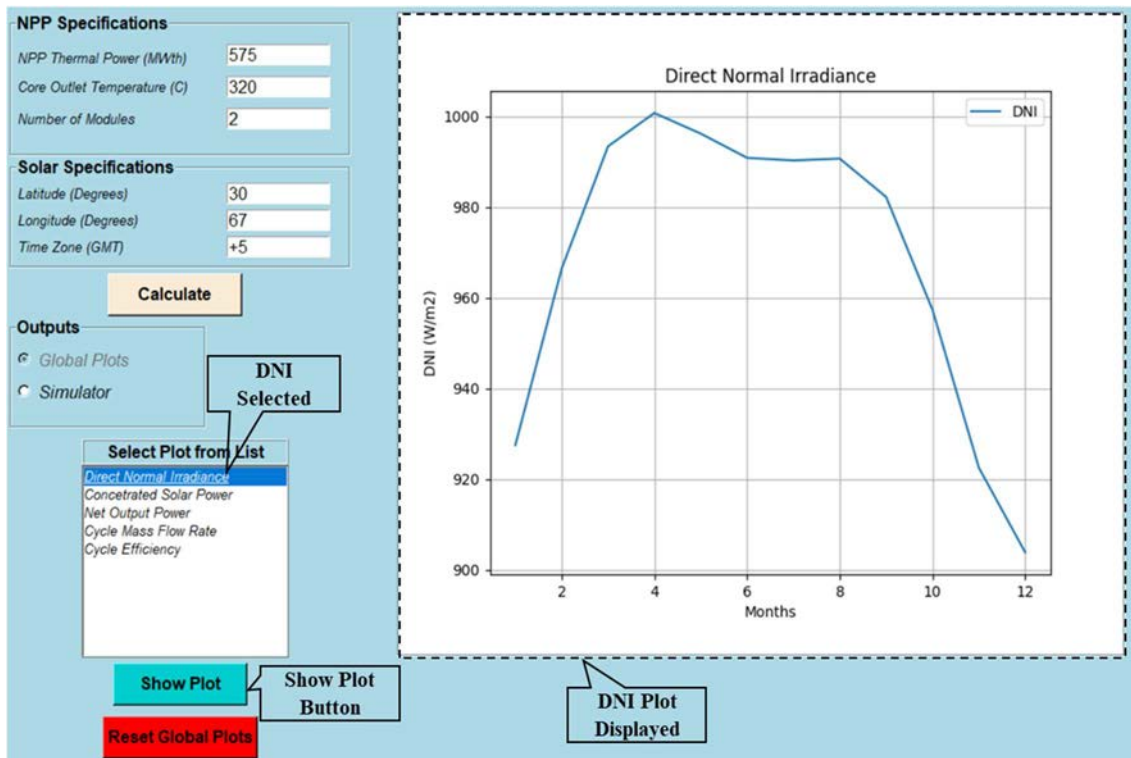


FIG. 6. Nuclear-solar HES part-task simulator: global plots mode example - plot of direct normal irradiance.

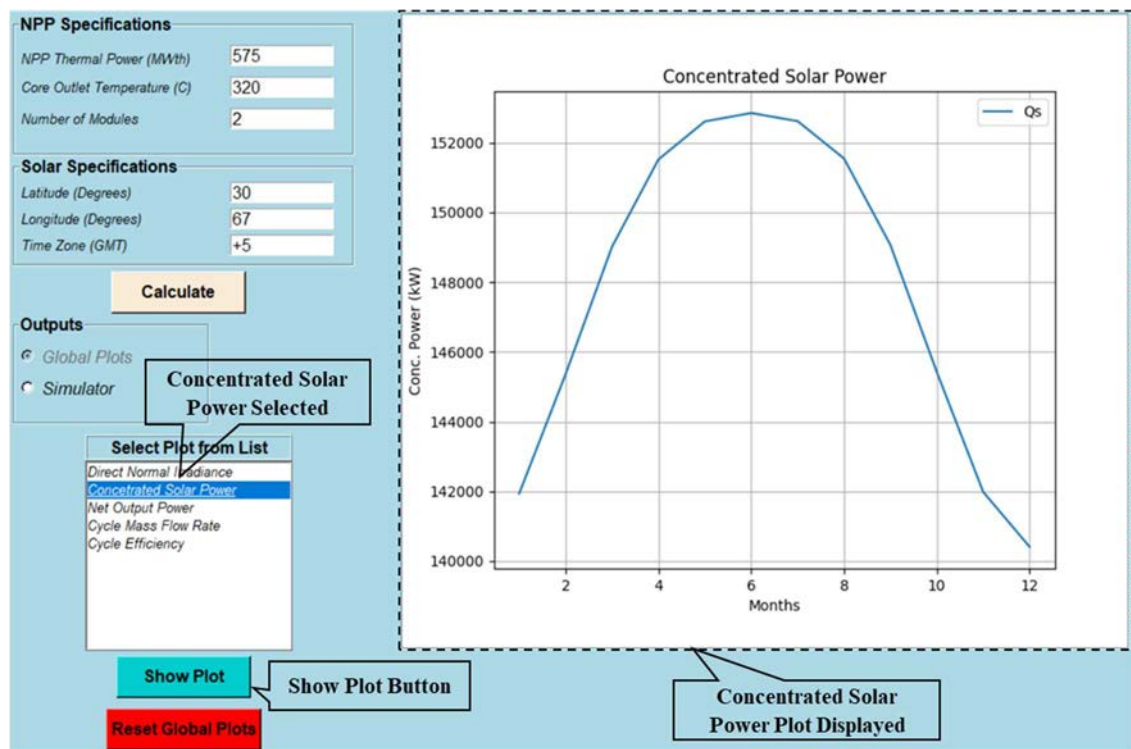


FIG. 7. Nuclear- solar HES part-task simulator: global plots mode example – plot of concentrated power.



Similarly, yearly variation of concentrated power can be obtained by selecting “Concentrated Power” from the list and clicking “Show Plot” button, as shown in FIG. 7. In a similar way, yearly variation plots of net output power, cycle mass flow rate and cycle efficiency can be obtained.

### 3.3.2. Simulator mode

This mode is selected by clicking on the option below “Global Plots”, FIG. 8. “Simulator” mode enables user to visualize oscillating responses of the HES at a particular time in a year. Schematics diagram for the coupling of CSP plant with secondary side of a NPP is as well displayed. At any time, the mode can be switched from “Simulator” to “Global Plots” and vice versa.

Two graphs will be displayed as shown in FIG. 9 based on NPP and solar specifications initially provided, as shown in FIG. 4. These graphs allow to visualize variations in electric power from CSP plant as well as net power output during certain time span in the year. The user can also zoom in using the “Span” slider. The  $x$  axes of the graphs represent the hours of the year (with maximum limit as the total number of hours in all days in a year). The  $x$  axes values can be selected using “Select Hour of the Year” slider value exactly in center of the  $x$  axis. The number of hours shown in  $x$  axes are controlled by the value selected using the “Select Span of the Graph” slider. The  $y$  axis represents the concentrated power obtained from CSP plant whereas the  $y$  axis of a second graph represents the net power output of the complete HES.

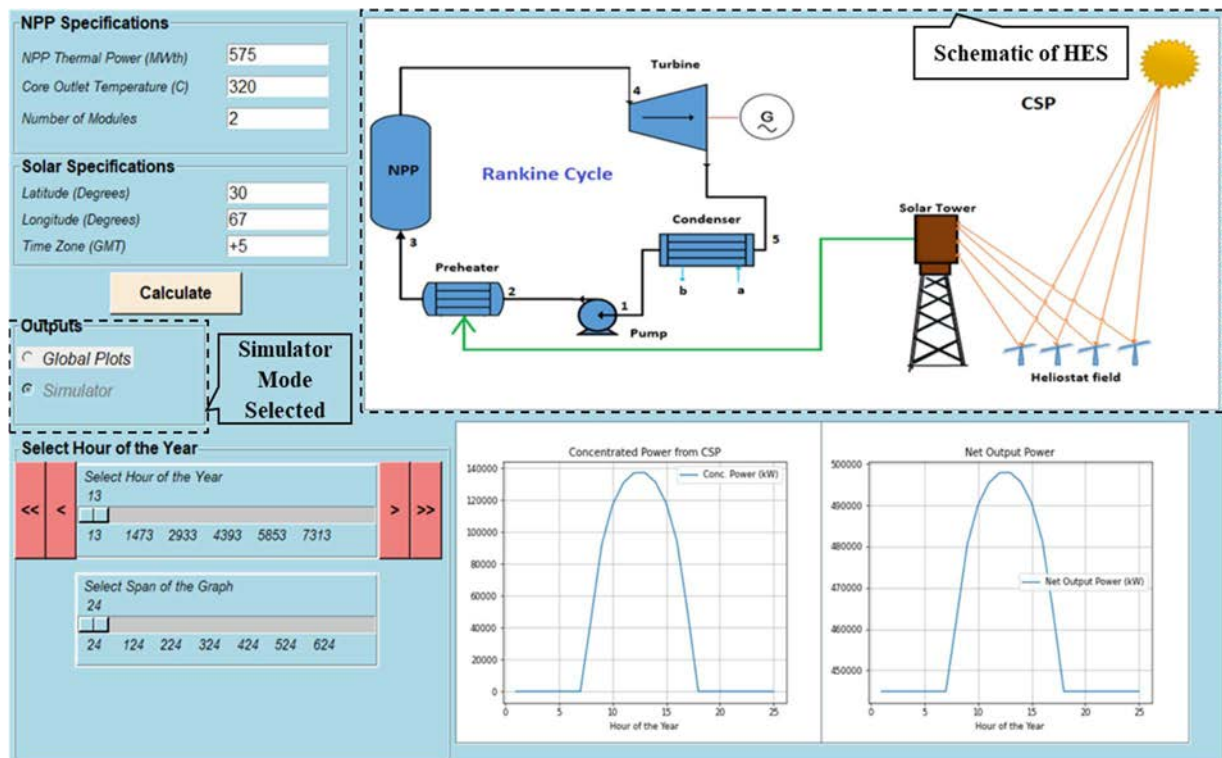


FIG. 8. Nuclear-solar HES part-task simulator: simulator mode.

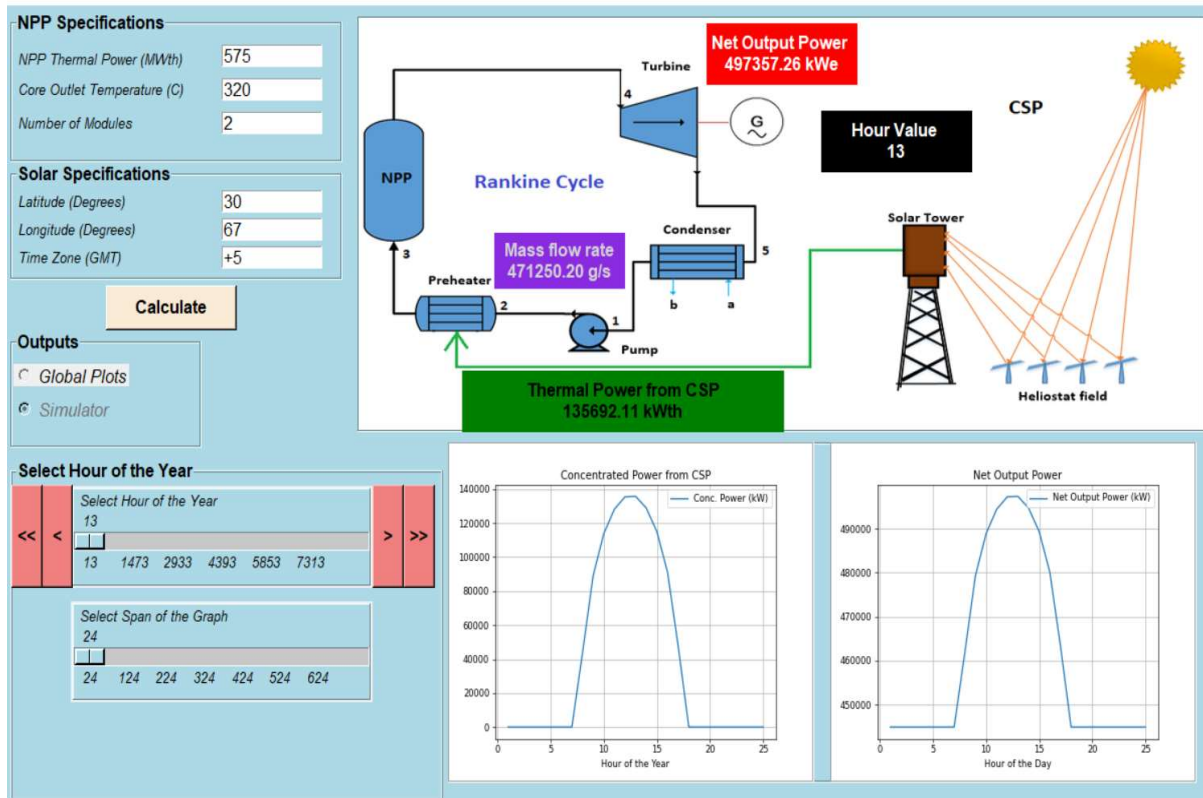


FIG. 9. Nuclear-solar HES part-task simulator: simulator mode outputs.

## 4. EXAMPLES

All figures in this publication are screen shots of the simulator display and plots generated by the nuclear-solar HES part-task simulator in addition to other illustrations. The following are the examples workable for self-learning and to be used in education and training workshops.

### 4.1. MONTHLY POWER VARIATION (GLOBAL PLOTS MODE)

Monthly variation of direct normal irradiance, CSP, HES total power output, cycle mass flow rate and the cycle efficiency are studied in this example. FIG. 10 shows schematics of relative position of earth with respect to sun and seasons in northern hemisphere. During the summer the earth is near the farthest point from the sun (aphelion) but tilted towards it, whereas during the winter it is near the nearest point from the sun (perihelion) but tilted away from it. Because of the earth tilt, northern hemisphere receives larger amount of sunlight during the summer as compared to winter (i.e., the days during the summer are relatively longer when compared to winter at the same location on earth in northern hemisphere). The opposite is true for the southern hemisphere. At equinoxes (both spring and autumn) the length of days and nights are almost the same, and the opposite location on earth receives almost equal amount of sunlight in northern as well as southern hemisphere. In this example, monthly variation of output parameters for nuclear-solar HES part-task simulator is studied incorporating relative position of the earth around the sun and seasonal variations (earth tilt). The location of CSP plant on earth is shown as point 'a' (FIG. 10) at 30° latitude and 67° longitude at +5 GMT.

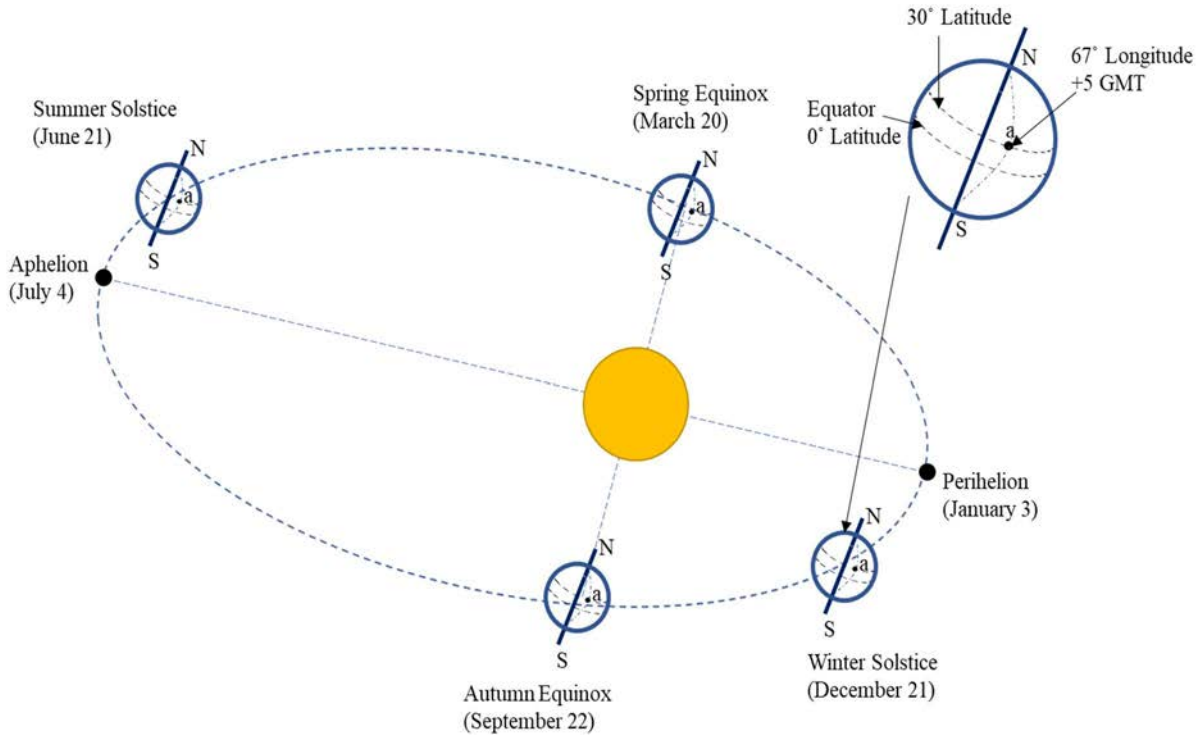


FIG. 10. Relative position of earth with respect to sun throughout the year used in the example on monthly power variation.

#### 4.1.1. Simulation steps

In Step 1, run the nuclear-solar HES part-task simulator by clicking the ‘Start’ button and wait until the simulator is initialized. The simulator is initialized with some default input values. In Step 2, Change “NPP Thermal Power” from 575 MWth to 347 MWth, and “Number of Modules” from 2 to 1. Keep the remaining inputs to default values. In Step 3, click on the “Calculate” button as shown in FIG. 4. This will calculate the output parameter values for the global plot mode. In Step 4, select the “Direct Normal Irradiance” from the list of plots and then click on “Show Plot” (FIG. 11). In Step 5, click on the “Reset Global Plots” button to remove the current graph. Repeat step 4 and 5 for all output parameter to visualize the graphs as shown in FIG. 12 to FIG. 15.

#### 4.1.2. Analysis of the output parameters

FIG. 11 shows the monthly variation of direct normal irradiance on clear sunny days at the specified latitude, longitude, and time zone. It is the most important aspect in assessing the power output of CSP plant and depends on geographic location, time of the day, season, and the earth’s location in the elliptical orbit around the sun. The specified location lies in the northern hemisphere (30° latitude, 67° longitude), for which the winter solstice is in month of December meaning that northern hemisphere is tilted away from the sun. Additionally, the earth will be at perihelion in January. The minimum value of direct normal irradiance should be in these months. The graph shows that the value of direct normal irradiance is minimum in December. The end of March is the spring equinox in northern hemisphere. During this period



sunlight is directly hitting the equator and the earth is moving away from perihelion, which results in maximum direct normal irradiance at the end of March or beginning of April. The summer solstice occurs in June, which means the northern hemisphere is tilted towards the sun. But the earth is near the aphelion during this month. Thus, the combined effect is the small decrease in direct normal irradiance value. The value increases by small amount as the earth is moving towards the autumn equinox (September) and away from aphelion. The value of direct normal irradiance starts to decrease again as the earth moves towards perihelion and winter solstice.

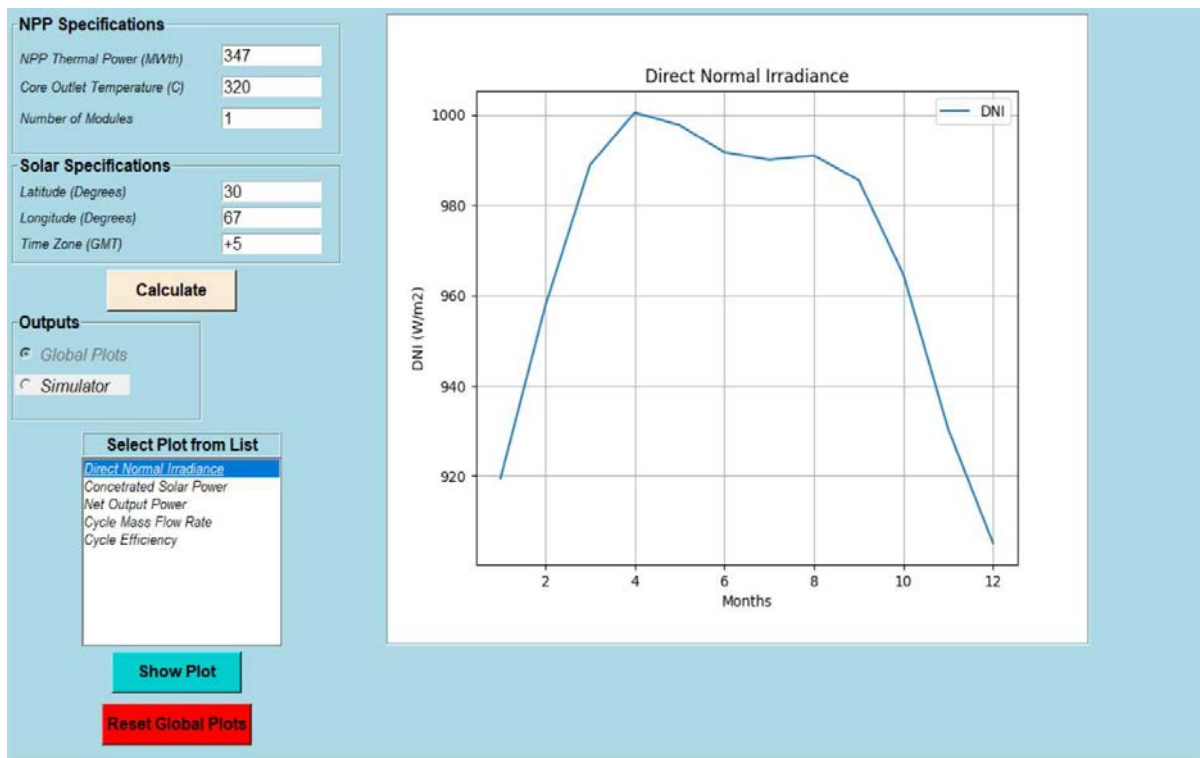


FIG. 11. Nuclear-solar HES part-task simulator: direct normal irradiance for the example on monthly power variation (global plots mode).

FIG. 12 shows monthly variation of concentrated solar power at the solar power tower after incorporating the effects of atmospheric mass, size and number of heliostats, shape of heliostats, and atmospheric turbidity in direct normal irradiance. The CSP plant is producing maximum power during the summer and minimum power during the winter at specified location in the northern hemisphere. The minimum power output from CSP plant is 139 MWth in December, whereas peak power output from CSP plant is 151 MWth in June. The heliostat field used in calculating the CSP is shown in FIG. 2 and the total number of mirrors of 1856 is a fixed value.

FIG. 13 shows the net power output from the HES which is the total electrical power output from the nuclear-solar HES. The trend for net power output is exactly similar to the one obtained for power output of CSP plant because the SMR is always operating at constant power. The minimum net power output from HES is 188 MWe in December, whereas the maximum net power output from HES is 193 MWe in June.

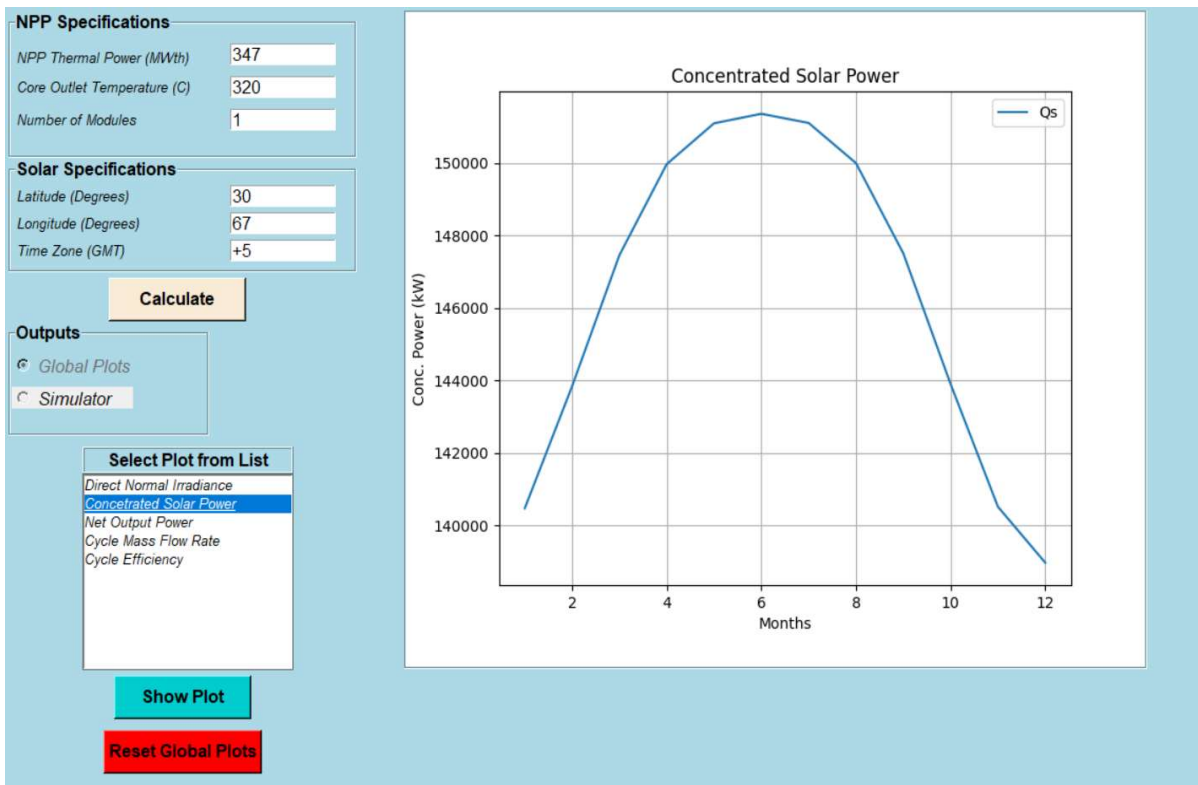


FIG. 12. Nuclear-solar HES part-task simulator: concentrated solar power for the example on monthly power variation (global plots mode).

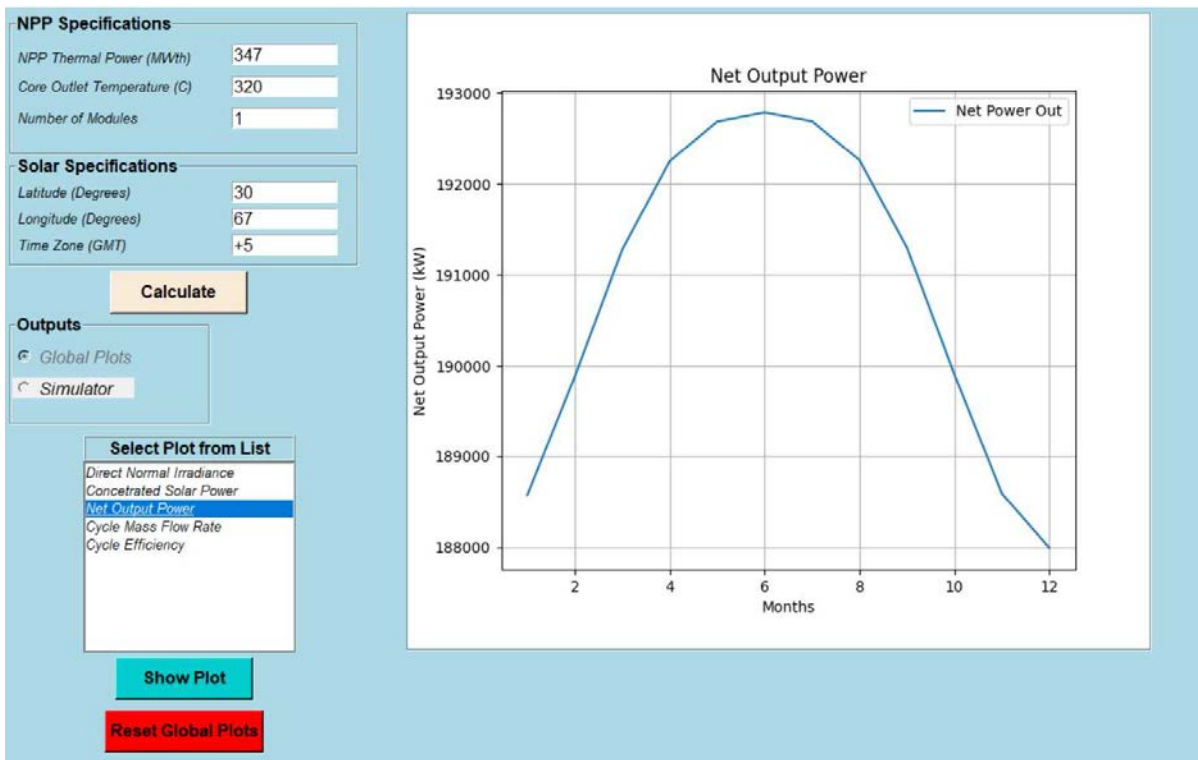


FIG. 13. Nuclear-solar HES part-task simulator: net output power for the example on monthly power variation (global plots mode).

The cycle mass flow rate also follows exactly the similar trend (as shown in FIG. 14). With increase of power output from CSP plant (FIG. 12), there is more amount of heat that is being added in the Rankine cycle. This addition of heat, if at constant mass flow rate, causes increase in temperature at the turbine inlet, which is assumed to be fixed in this example. Thus, the mass flow rate must increase in order to carry the energy from the preheater to steam generator and then to the turbine inlet. The increase in mass flow rate increases the amount of heat transfer and the net amount of the electrical power produced at the generator.

The variation in mass flow rate is between 178 kg/s and 183 kg/s throughout the year. However, this monthly variation does not account for the night time during the month and hence does not represents the average value. Better variation in mass flow rate can be obtained by incorporating the hourly variation (as discussed in Section 4.2).

The efficiency of the Rankine cycle remains constant throughout the year as can be seen in FIG. 15, which is 38.6 % because of the fixed turbine inlet temperature. The Rankine cycle efficiency can only vary if the temperature at the turbine inlet or the outlet changes in this case. The part-task simulator takes sum of the thermal power from both the SMR and CSP plant as the input thermal power available.

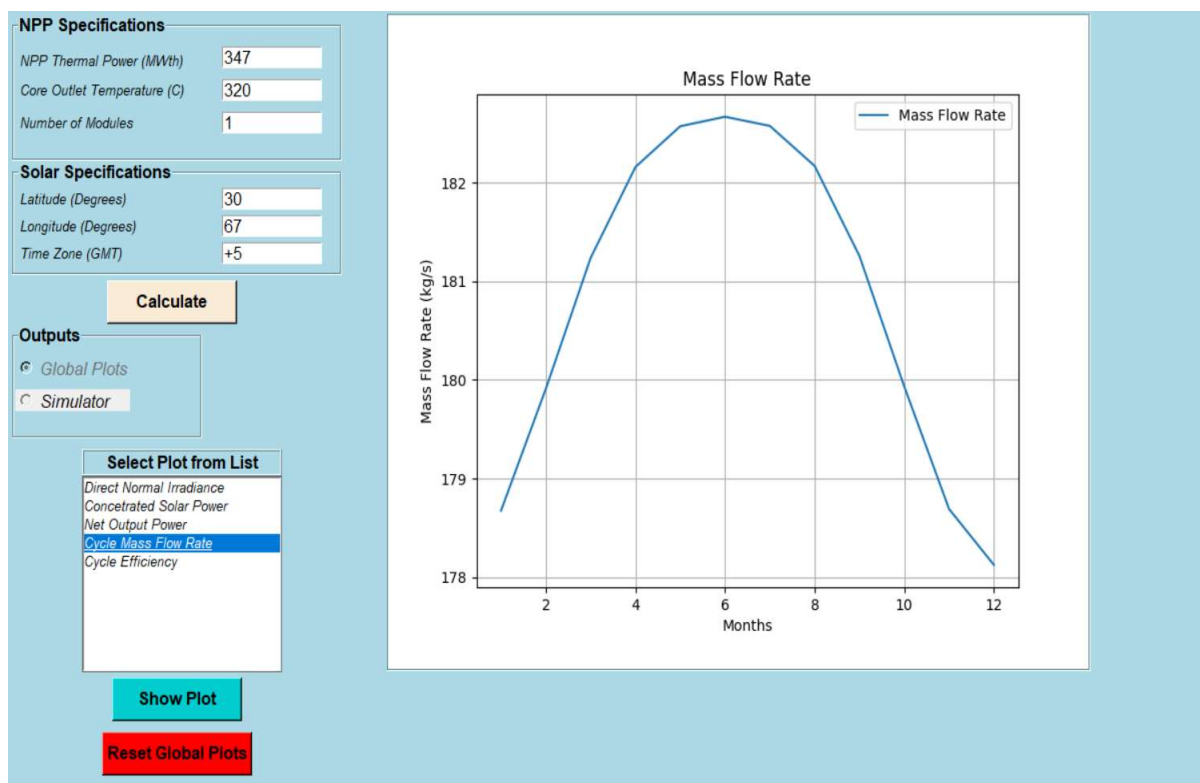


FIG. 14. Nuclear-solar HES part-task simulator: cycle mass flow rate for the example on monthly power variation (global plots mode).

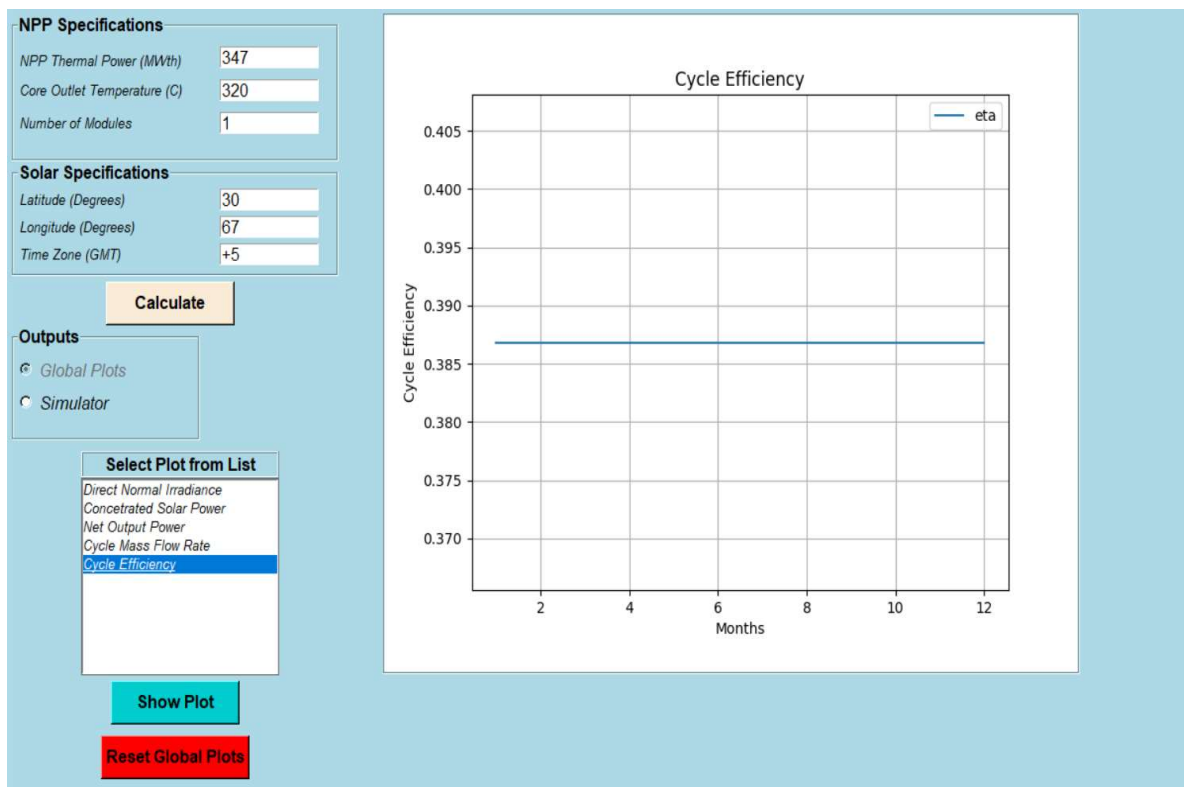


FIG. 15. Nuclear-solar HES part-task simulator: cycle efficiency for the example on monthly power variation (global plots mode).

## 4.2. HOURLY POWER VARIATION (SIMULATOR MODE)

To visualize the hourly variation, nuclear-solar HES part-task simulator is operated in ‘Simulator’ mode. This mode is developed to incorporate the hourly position as well as monthly position of the sun relative to earth. The part-task simulator calculates the power at the CSP plant and the net output power from the HES in one complete year.

### 4.2.1. Simulation steps

Repeat Step 1 to Step 3 described in Section 4.1.1. In Step 4, click on the “Simulator” button positioned below “Global plots” as shown in FIG. 8. A new window will open asking to wait until the calculations are complete. This is shown in FIG. 16. In Step 5, close the calculation progress window after the graphs appear on the main window as it can be seen in FIG. 17. In Step 6, set the “Select Hour of the Year” slider to 23 by clicking on “>>” button, which will increment the hour value by 10 and keep the “Select Span of the Graph” slider to its default value (i.e., 24). The obtained graph is shown in FIG. 18. In Step 7, drag the “Select Hour of the Year” slider to 3185 hour, and the “Select the Span of the Graph” slider to 332 as shown in FIG. 19.

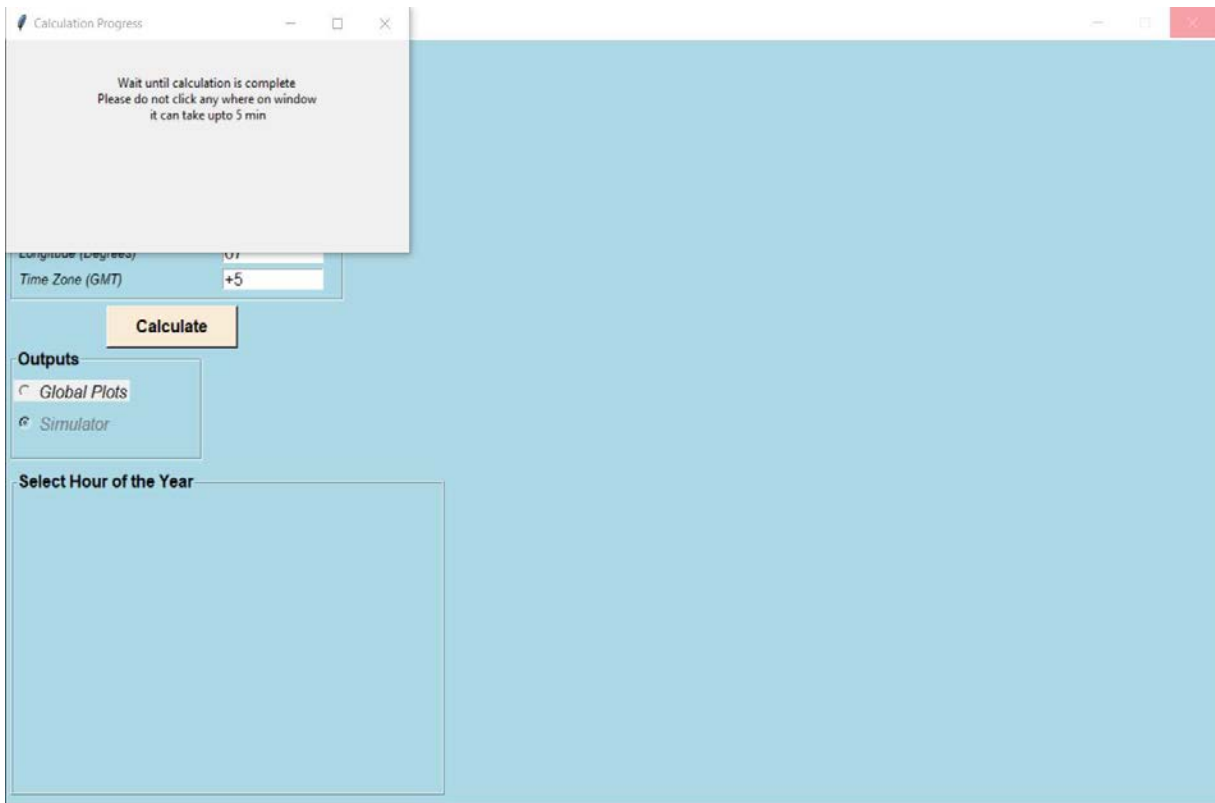


FIG. 16. Nuclear-solar HES part-task simulator: simulator mode calculation in progress.

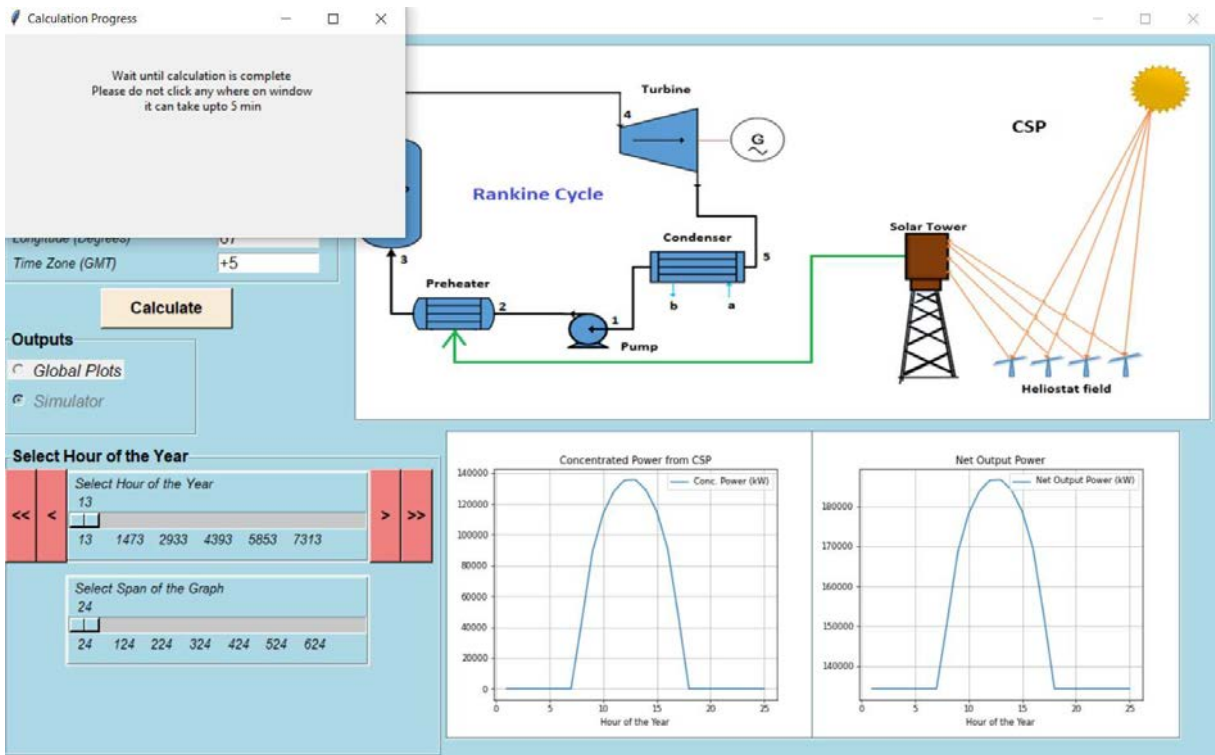


FIG. 17. Nuclear-solar HES part-task simulator: simulator mode calculations completed.

#### 4.2.2. Analysis of the output parameters

FIG. 18 shows the nuclear-solar HES part-task simulator output parameters for the specified inputs. The graph at the bottom left side represents the hourly variation of the concentrated solar power in kWth, and the graph at the bottom right side represents total power from the HES in kWe. The CSP plant power output between hour 18 to 31 (1 January from 6 pm to 2 January to 7 am) is zero, because it is a nighttime at the specified location and the HES does not incorporate any electrical power storage device. During this time, the total electrical output is only from SMR, i.e, 131 MWe (38% of 347 MWth). As the sun starts to rise after hour 31 (2 January at 7 am), the thermal power output from CSP plant starts to increase, which results in an increase in total power output from the whole HES. The peak power output from CSP plant on 1 January is 135 MWth. The schematic at the top shows the values of thermal power from CSP plant, cycle mass flow rate, the net output power of the HES and the hour value at which values are displayed. At 23<sup>rd</sup> hour, the thermal output power from CSP plant is zero, whereas the total power output is 134.2 MWe and the mass flow rate is 127 kg/s.

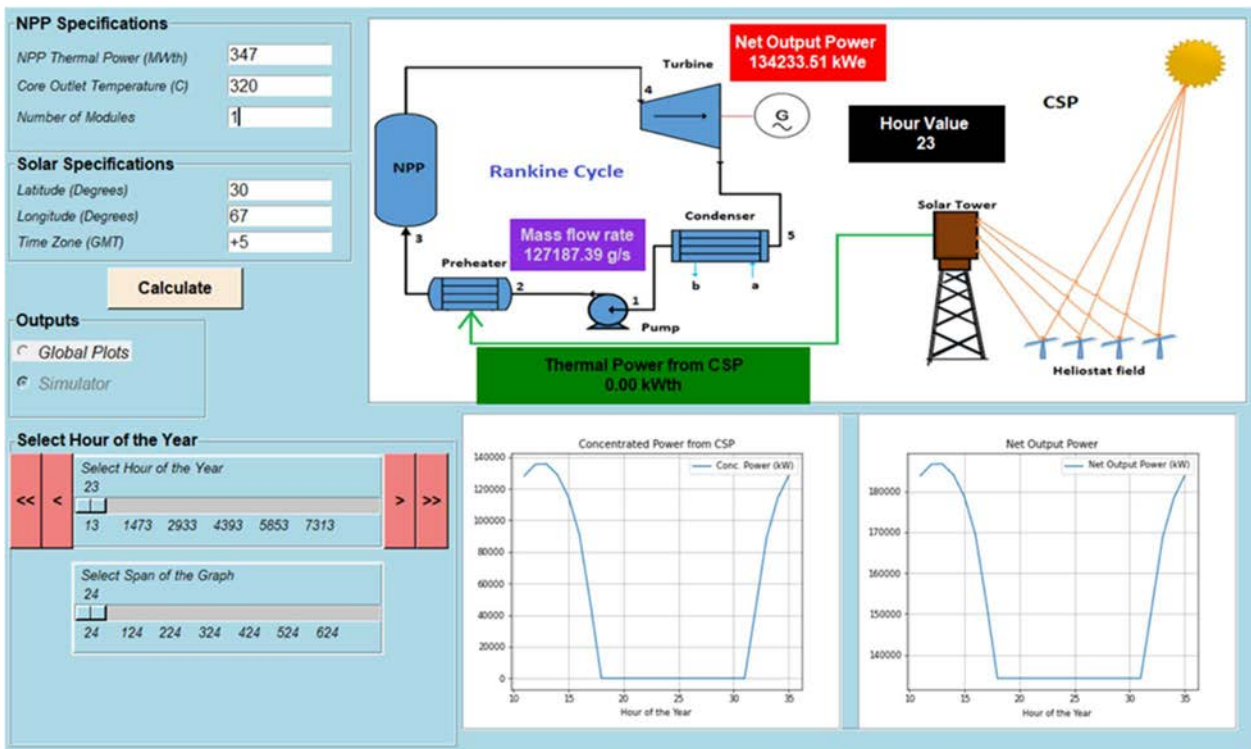


FIG. 18. Nuclear-solar HES part-task simulator: output parameters for the example on hourly power variation (simulator mode).

FIG. 19 shows the output of HES at 3185<sup>th</sup> hour. The span of the graph is set to 720 and the graphs show the hourly variation for one complete month (720 hours). Because of the simplified models the total output power exactly follows the CSP curve. The peak on the graph at bottom left shows that the maximum CSP is near 160 MWth, whereas the total peak electrical output power is 195 kWe, although the SMR used 347 MWth. This is because of Rankine cycle thermal efficiency of 38%. The peak electrical power is 38% of total thermal power from both SMR and CSP plant. The cycle mass flow rate at this hour is 170.5 kg/s.



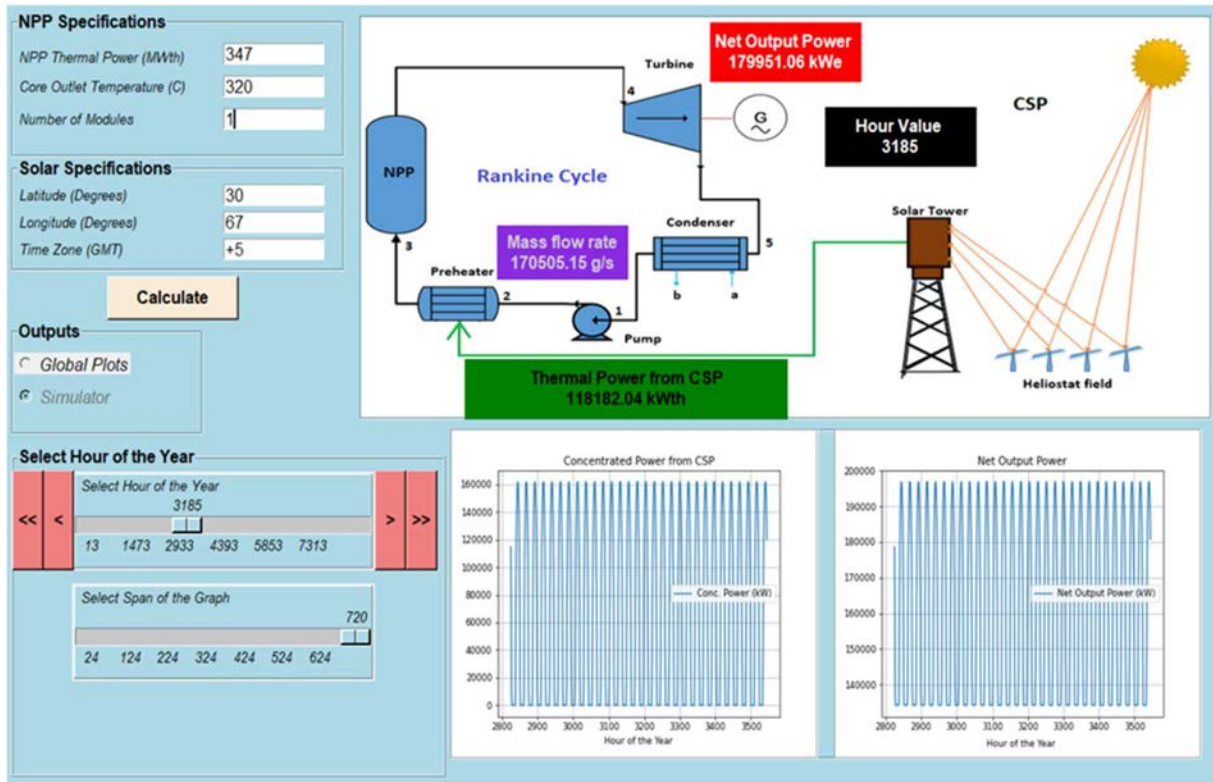


FIG. 19. Nuclear-solar HES part-task simulator: values of output parameters at 3185<sup>th</sup> hour of the year for the example on hourly power variation (simulator mode).

#### 4.3. EFFECT OF LATITUDE ON OUTPUT PARAMETERS (GLOBAL PLOTS MODE)

In this example different latitude values are used and the part-task simulator is run in its “Global Plots” mode.

##### 4.3.1. Simulation steps

This simulation follows the same steps as described in Section 4.1.1 except for changing “Latitude” to  $-30$ .

##### 4.3.2. Analysis of the output parameters

FIG. 20 shows monthly variation of direct normal irradiance in southern hemisphere. The trend is completely opposite to that in the northern hemisphere (compare to FIG. 11). This is because of seasonal variations in the southern hemisphere that is completely opposite to that in the northern hemisphere. The maximum direct normal irradiance is in month of December (Perihelion + tilt towards the sun) whereas minimum direct normal irradiance is in June (aphelion + tilt away from the sun).

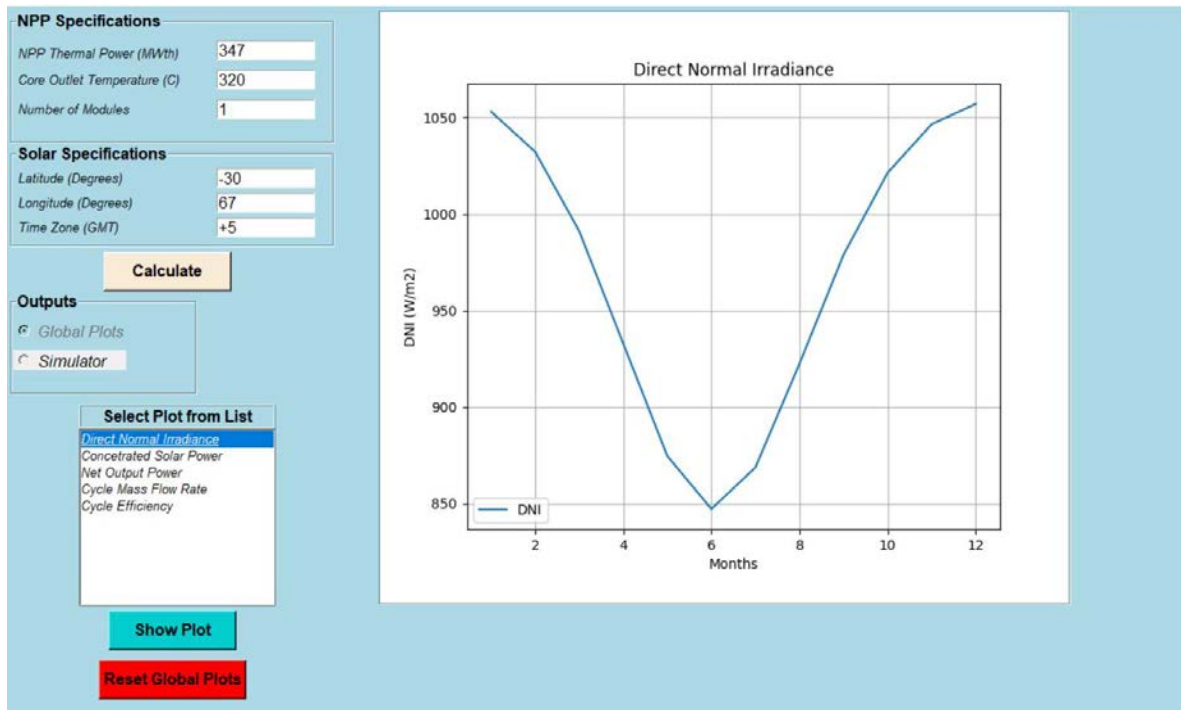


FIG. 20. Nuclear-solar HES part-task simulator: direct normal irradiance in southern hemisphere (global plots mode).

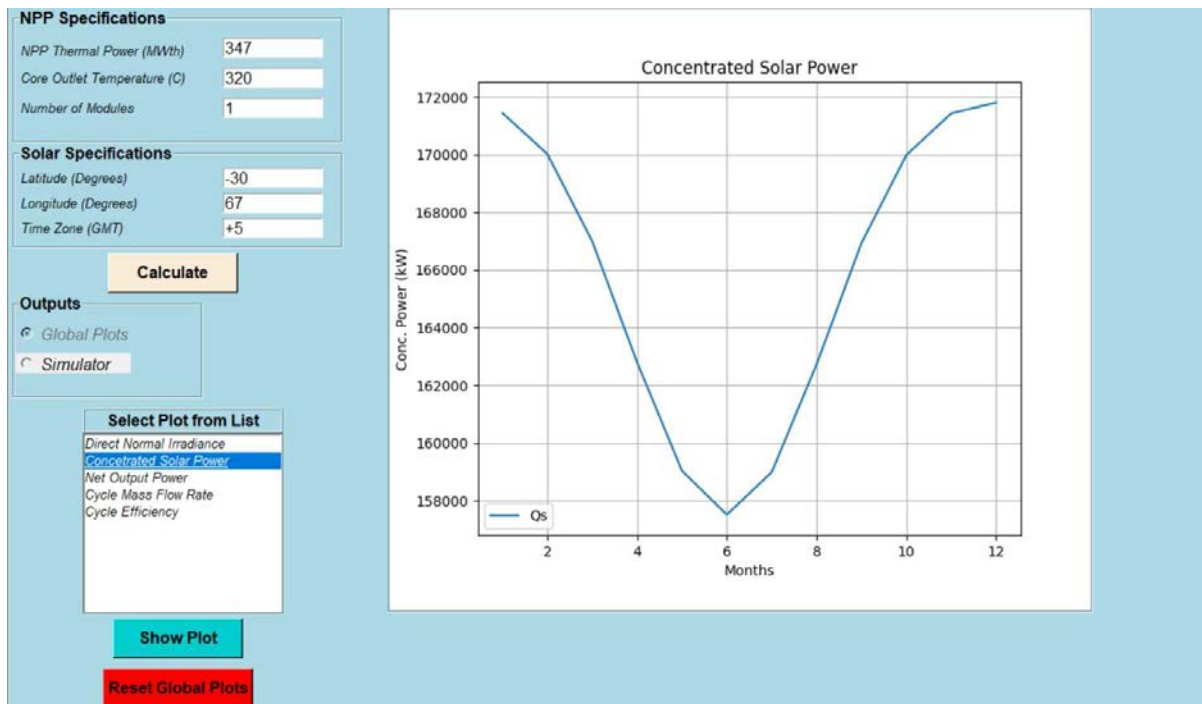


FIG. 21. Nuclear-solar HES part-task simulator: concentrated solar power in southern hemisphere (global plots mode).

FIG. 21 shows monthly variation of the concentrated solar power at the specified location which exactly follows direct normal irradiance. The minimum concentrated solar power is 158 MWth during the month of June whereas the maximum concentrated solar power is about 172 MWth during December. The net power output and cycle mass flow rate from the nuclear-solar HES



follows similar pattern to that of direct normal irradiance as shown in FIG. 22 and FIG. 23, respectively. The peak net power output and minimum power output is 201 MWe and 195 Mwe, respectively. The cycle mass flow rate varies between 185 kg/s and 190 kg/s.

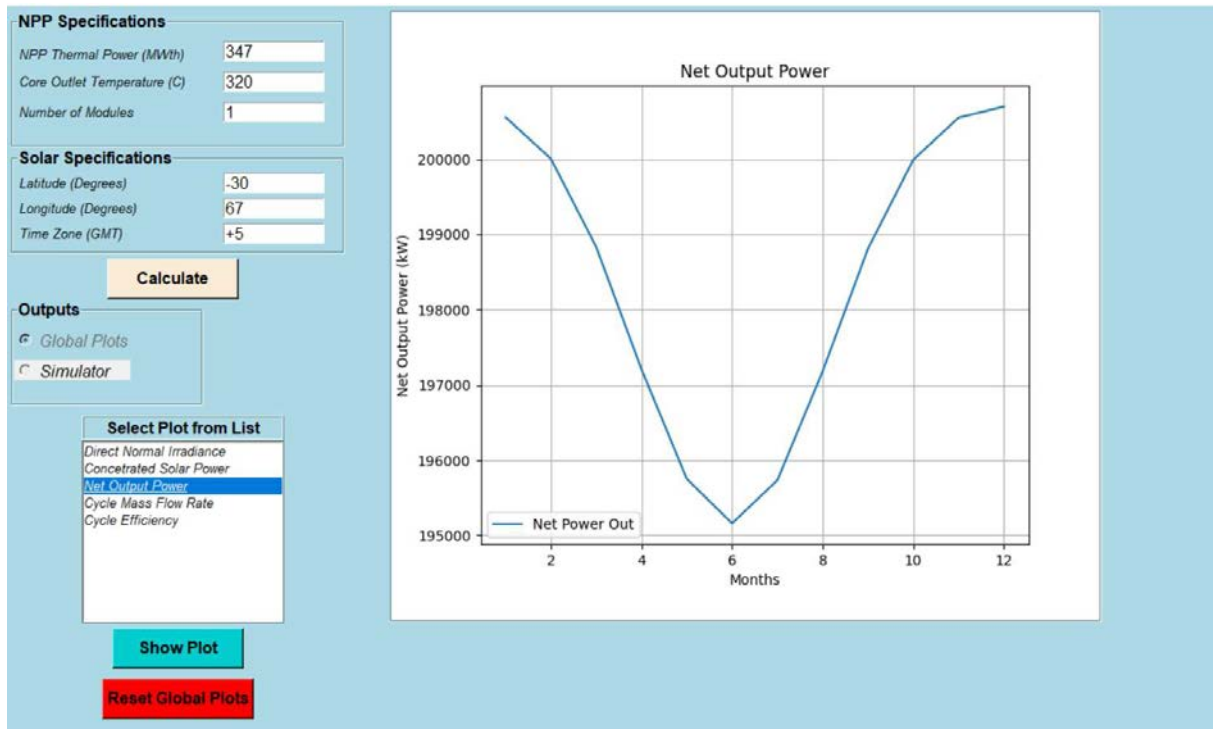


FIG. 22. Nuclear-solar HES part-task simulator: total power output in southern hemisphere (global plots mode).

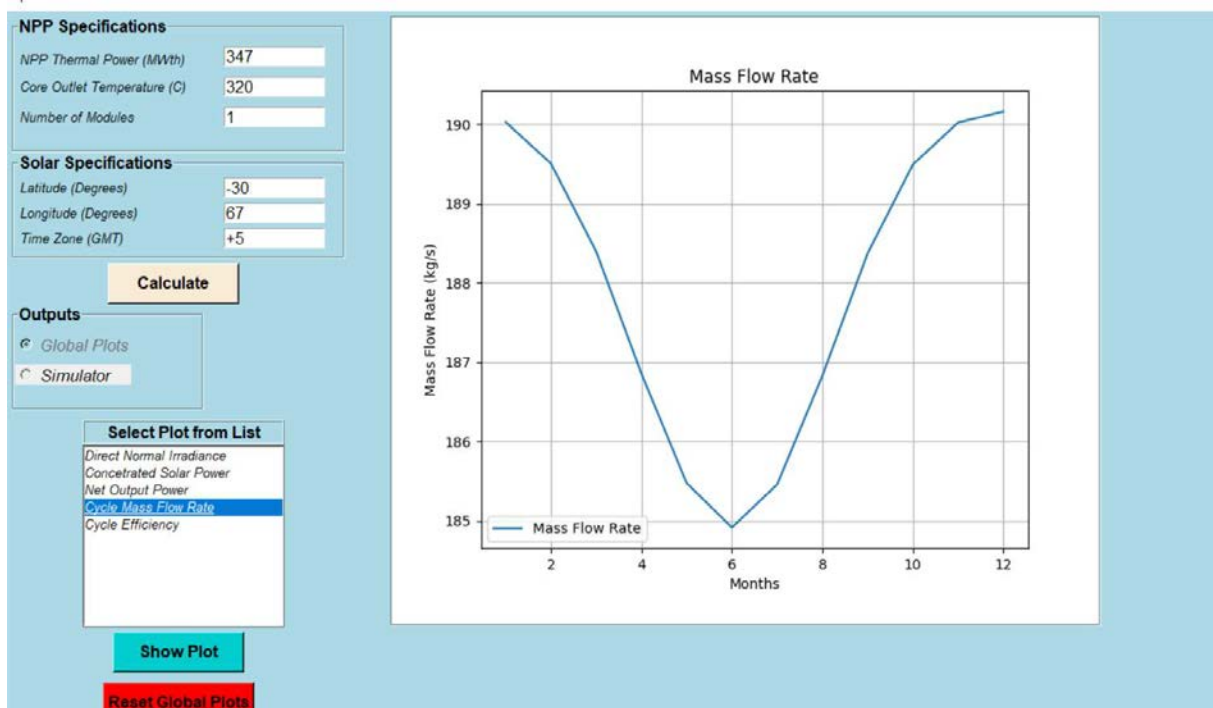


FIG. 23. Nuclear-solar HES part-task simulator: cycle mass flow rate in southern hemisphere (global plots mode).

#### 4.4. EFFECT OF CORE OUTLET TEMPERATURE ON CYCLE MASS FLOW AND EFFICIENCY (GLOBAL PLOTS MODE)

In this example, the “Global Plots” mode is used to study the effects of different core outlet temperatures on cycle mass flow rate and efficiency. The values of direct normal irradiance, CSP, and net output power remains the same as described in Section 4.1.

##### 4.4.1. Simulation steps

Repeat the Step 1 and 2, as described in Section 4.1.1. In Step 3, change the “Core Outlet Temperature” from 320°C to 290°C and then click on calculate button (as shown in FIG. 24). In Step 4, select the “Cycle Mass Flow Rate” and then click on show plot to view the graph as shown in FIG. 25. In Step 5, click on “Cycle Efficiency” and then click on show plot to view the graph. In Step 6, click on “Reset Global Plots” to remove the current graphs. Repeat Step 3 to Step 6 for “Core Outlet Temperature” of 300°C and 310°C.

The screenshot displays the input parameters for the Nuclear-solar HES part-task simulator. It is divided into several sections:

- NPP Specifications:** Includes input fields for NPP Thermal Power (MWth) set to 347, Core Outlet Temperature (C) set to 290, and Number of Modules set to 1.
- Solar Specifications:** Includes input fields for Latitude (Degrees) set to 30, Longitude (Degrees) set to 67, and Time Zone (GMT) set to +5.
- Calculate:** A yellow button to execute the simulation.
- Outputs:** A section with radio buttons for "Global Plots" (selected) and "Simulator".
- Select Plot from List:** A dropdown menu showing a list of available plots: Direct Normal Irradiance, Concentrated Solar Power, Net Output Power, Cycle Mass Flow Rate, and Cycle Efficiency.
- Show Plot:** A blue button to display the selected plot.
- Reset Global Plots:** A red button to clear the current plots.

FIG. 24. Nuclear-solar HES part-task simulator: input parameters for the example of the effect of core outlet temperature on cycle mass flow rate and efficiency (global plots mode).

#### 4.4.2. Analysis of the output parameters

FIG. 25 shows the variation of cycle mass flow rate for 290°C core outlet temperature. Although the SMR thermal power and the location of CSP plant is the same as used in the example described in Section 4.1, the values of cycle mass flow rate are different.

The cycle mass flow rate is higher in this case because the thermal power from SMR and CSP plant are still the same as in the example described in Section 4.1, but the core outlet temperature is decreased, thus the high mass flow rate is required to transfer the same amount of thermal power. The peak value of cycle mass flow rate is 193 kg/s in June whereas the minimum value of cycle mass flow rate is 188 kg/s in December.

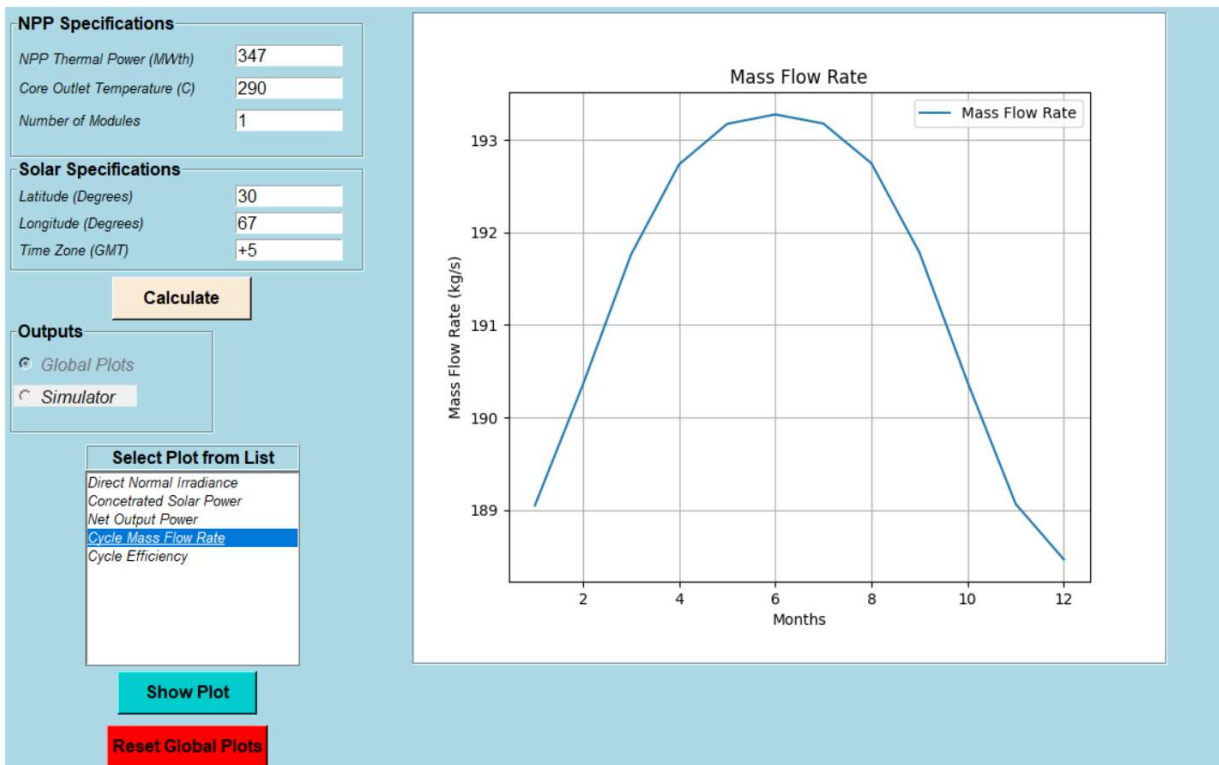


FIG. 25. Nuclear-solar HES part-task simulator: cycle mass flow rate at 290°C for the example on effect of core outlet temperature on cycle mass flow rate and efficiency (global plots mode).

FIG. 26 shows the cycle efficiency monthly variation for 290°C core outlet temperature. The cycle efficiency is constant throughout the year (similar to the one shown in FIG. 15). However, the value of efficiency is reduced from 38.5% to 36.5% as the core outlet temperature is decreased from 320°C to 290°C, because the turbine inlet temperature is decreased from 310°C to 280°C.

It is assumed that the pinch point temperature difference for the steam generator is 10°C (as shown in TABLE 1). Thus, the turbine inlet temperature varies only with core outlet temperature.

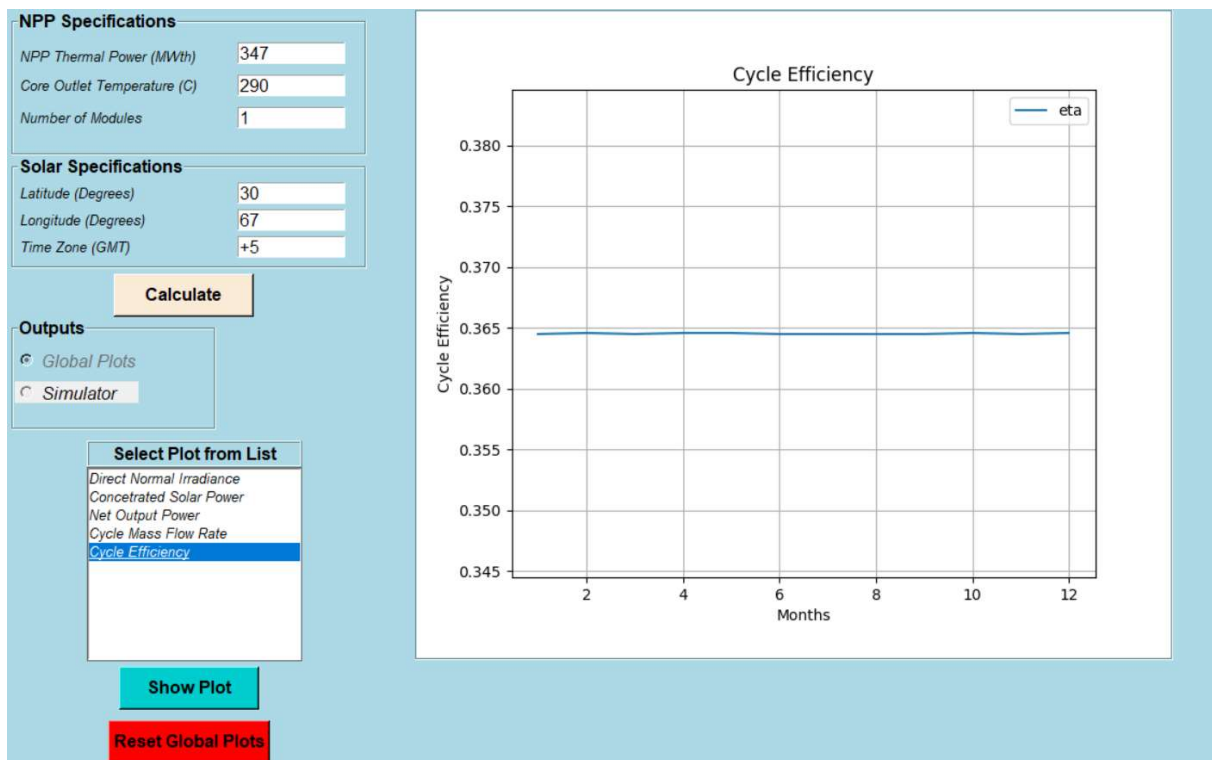


FIG. 26. Nuclear-solar HES part-task simulator: cycle efficiency at 290°C for the example on effect of core outlet temperature on cycle mass flow rate and efficiency (global plots mode).

TABLE 2 shows the values of minimum cycle mass flow rate, peak cycle mass flow rate and the cycle efficiency for three different core outlet temperatures. The cycle mass flow rate decreases with increase of a core outlet temperature, whereas cycle efficiency increases with increase of a core outlet temperature.

TABLE 2. NUCLEAR-SOLAR HES PART-TASK SIMULATOR: OUTPUT PARAMETER VALUES FOR THE EXAMPLE ON EFFECT OF CORE OUTLET TEMPERATURE ON CYCLE MASS FLOW RATE AND EFFICIENCY

Core Outlet Temperature (°C)	Peak Cycle Mass Flow Rate (kg/s)	Minimum Cycle Mass Flow Rate (kg/s)	Cycle Efficiency (%)
290	194	188	36.4
300	189	184	37.4
310	186	182	38.1

#### 4.5. EFFECT OF LONGITUDE AND TIME ZONE ON DIRECT NORMAL IRRADIANCE (GLOBAL PLOTS MODE)

In this example, the effect of longitude and time zone on direct normal irradiance is analyzed. FIG. 27 shows the position of the earth relative to sun and the position of nuclear-solar HES at two different locations: point 'a' at 30° longitude and 30° latitude, and point 'b' at 90° longitude and 30° latitude. The earth completes one revolution (360°) around its axis in 24 hrs, thus covering 15° longitude in one hour. For the same latitude, the direct normal irradiance at any

longitude remains the same (neglecting the atmospheric effects), as each point on the constant latitude line receives the same amount of solar radiation but with a time shift.

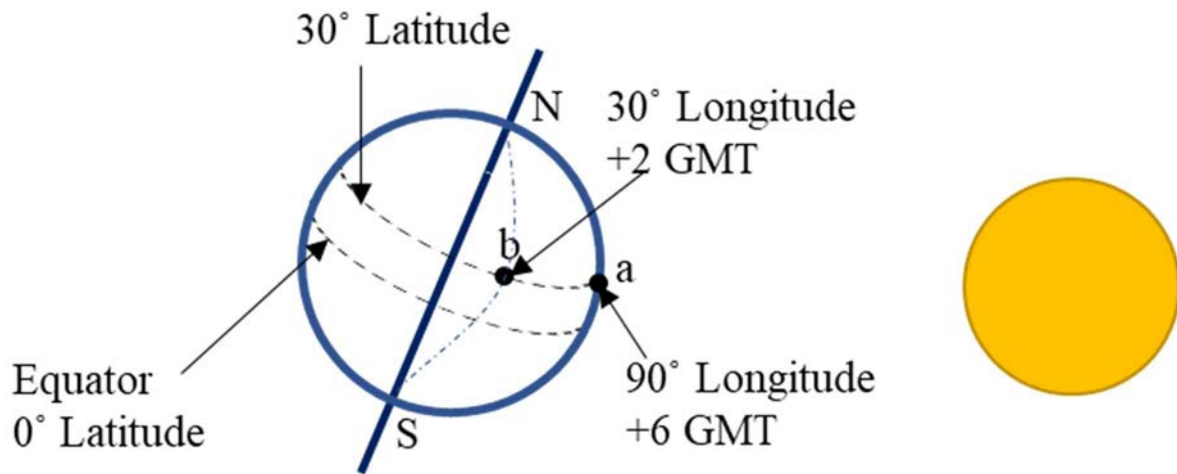


FIG. 27. Nuclear-solar HES part-task simulator: location of nuclear-solar HES at 30° and 90° longitudes for same latitude 30° (global plots mode).

#### 4.5.1. Simulation steps

This simulation using the “Global Plots” mode follows the same steps as described in Section 4.1.1. The only difference is in Step 2, in which the longitude value is changed to 30° and time zone to +2. Then click and plot the direct normal irradiance as shown in FIG. 28. As the additional step, change the longitude to 90° and time zone to +6. Run the simulation again to obtain direct normal irradiance as shown in FIG. 29.

#### 4.5.2. Analysis of output parameters

FIG. 28 shows monthly variation of direct normal irradiance at 30° latitude, 30° longitude and +2 GMT. The direct normal irradiance increases from minimum in month of December to maximum in month of April as the earth revolves around the sun. The variation of direct normal irradiance obtained for 30° latitude, 90° longitude and +6 GMT is exactly same throughout the year as shown in FIG. 29, because at constant latitude the sunlight received at any longitude throughout the day is same. Thus, changing the longitude does not affect the variation of direct normal irradiance at constant latitude.

The power output from CSP plant directly depends on direct normal irradiance. It remains same at two different locations on earth with same latitude. Hence, the other output parameters such as the total power output and efficiency of the nuclear-solar HES also remains the same. However, local climate conditions (humidity, air quality, turbidity etc.) can affect the direct normal irradiance at different longitudes, but the major factor affecting variation in direct normal irradiance, and the power output from CSP plant is the latitude.

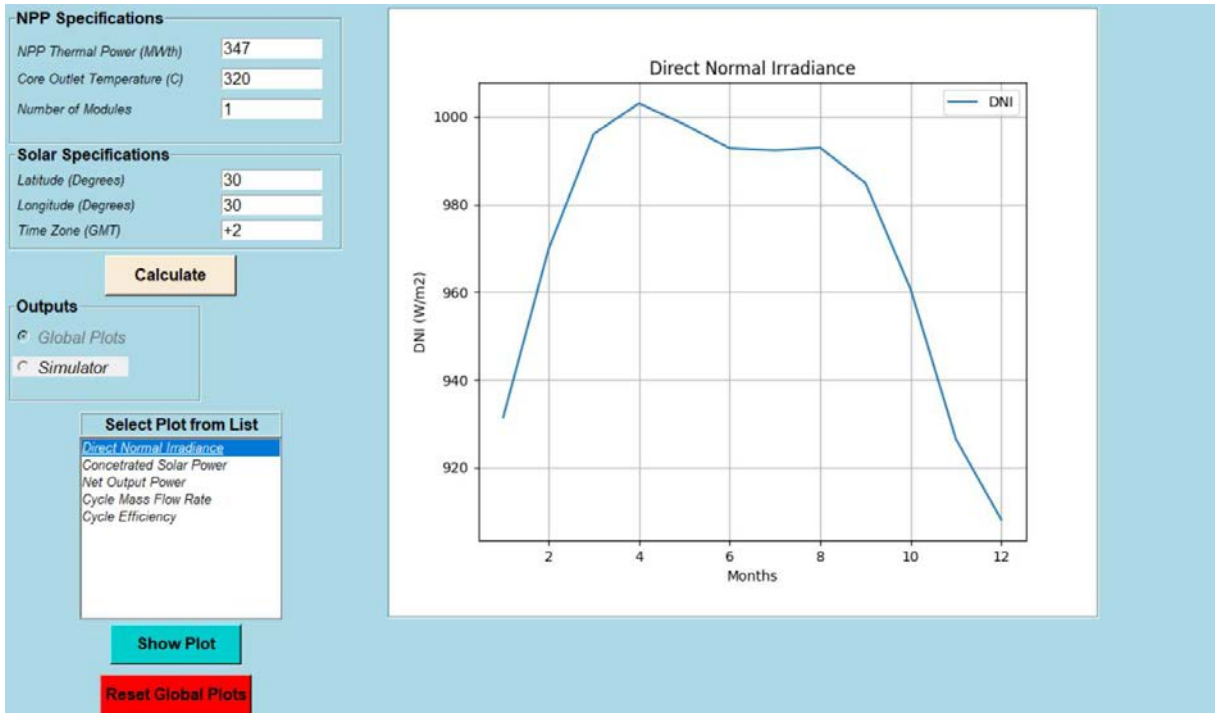


FIG. 28. Nuclear-solar HES part-task simulator: direct normal irradiance at 30° longitude and +2 GMT for the example of the effect of longitude and time zone on direct normal irradiance (global plots mode).

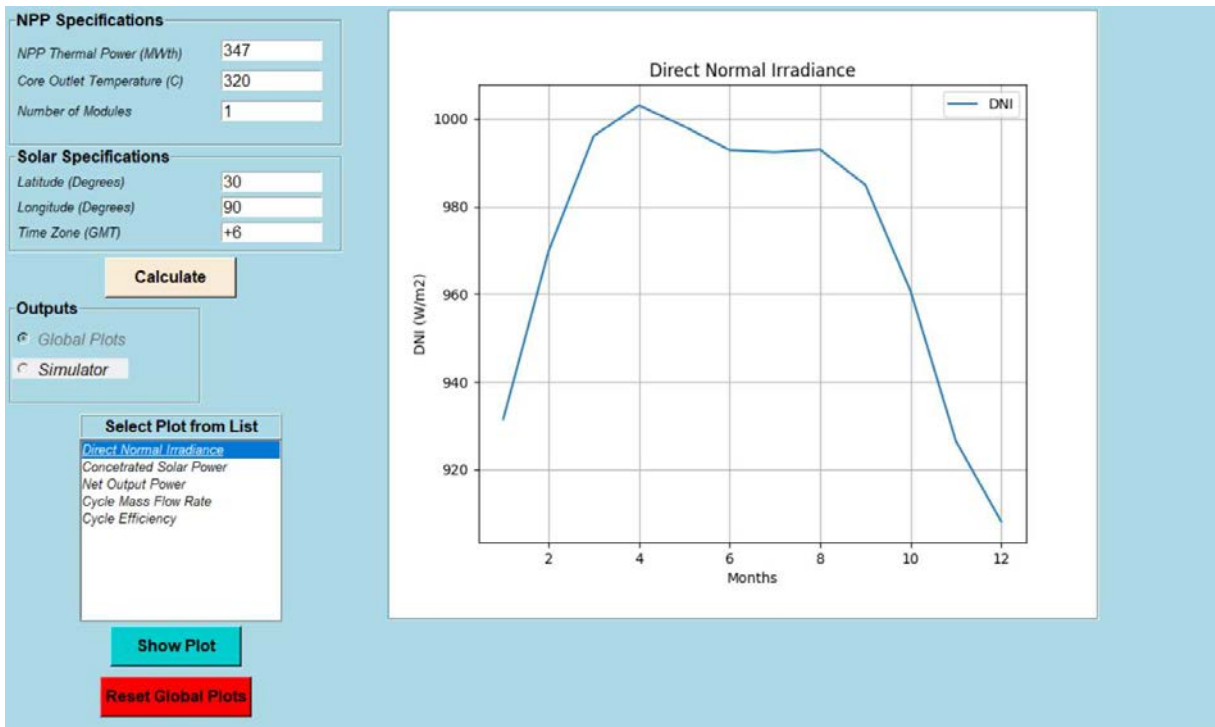


FIG. 29. Nuclear-solar part-task simulator: direct normal irradiance at 90° longitude and +6 GMT for the example of the effect of longitude and time zone on direct normal irradiance (global plots mode).



## REFERENCES

- [1] INTERNATIONAL ATOMIC ENERGY AGENCY, Classification, Selection and Use of Nuclear Power Plant Simulators for Education and Training, IAEA-TECDOC-1887, IAEA, Vienna (2019).
- [2] SUMAN, S., Hybrid nuclear-renewable energy systems: A review, *Journal of Cleaner Production* **181** 2018 166, 177.
- [3] INTERNATIONAL ENERGY AGENCY, Energy related CO<sub>2</sub> emissions, 1990-2019, IEA, Paris (2022). <https://www.iea.org/data-and-statistics/charts/energy-related-co2-emissions-1990-2019>
- [4] ZOHURI, B. *Small Modular Reactors as Renewable Energy Sources*, Springer, New York (2018).
- [5] INGERSOLL, D. T., et al., Can Nuclear Power and Renewables be Friends?, *Proceedings of ICAPP*, France (2015).
- [6] LOKHOV, A., Technical and Economic Aspects of Load Following with Nuclear Power Plants, NEA, OECD, Paris, France (2011).
- [7] INGERSOLL, D. T. (Eds), CARELLI, M. D. (Eds), *Handbook of Small Modular Nuclear Reactors*, Woodhead Publishing, UK (2020).
- [8] INTERNATIONAL ATOMIC ENERGY AGENCY, Advanced Reactor Information System (ARIS) Database. ARIS - Home ([iaea.org](http://iaea.org))
- [9] INTERNATIONAL ENERGY AGENCY, World Energy Balances, IEA, Paris (2021). <https://www.iea.org/data-and-statistics/charts/global-share-of-total-energy-supply-by-source-2019>
- [10] ALRIKABI, N.K., Renewable energy types, *Journal of Clean Energy Technologies* **2** 1 (2014) 61, 64.
- [11] DESIDERI, U., CAMPANA, P. E., Analysis and comparison between a concentrating solar and a photovoltaic power plant, *Applied Energy* **113** (2014) 422, 433.
- [12] BRAGG-SITTON, S. M., et al., Nuclear-Renewable Hybrid Energy Systems: 2016 Technology Development Program Plan, Idaho National Lab (INL), Rep. INL/EXT-16-38165, Idaho Falls, Oak Ridge, TN (United States) (2016).
- [13] INTERNATIONAL ATOMIC ENERGY AGENCY, Nuclear-Renewable Hybrid Energy Systems, IAEA-NR-T-1.24, IAEA, Vienna (2022).
- [14] BORISSOCA, A., POPOV, D., Analysis and Synthesis of Hybrid Nuclear-Solar Power Plants, Annual Conference of the Faculty of Power Engineering and Power Machines, Bulgaria (2015).
- [15] SON, I. W., et al., Feasibility study of solar-nuclear hybrid system for distributed power source, *Energy Conversion and Management* **230** (2021) 113808.
- [16] NOROUZI, N., FANI, M., TALEBI, S., Exergetic design and analysis of nuclear SMR reactor tetrageneration (combined water, heat, power, and chemicals) with designed PCM energy storage and a CO<sub>2</sub> gas turbine inner cycle, *Nuclear Engineering and Technology* **53** 2 (2021) 677, 687.
- [17] WANG, K., HE, Y. L., Thermodynamic analysis and optimization of a molten salt solar power tower integrated with a recompression supercritical CO<sub>2</sub> Brayton cycle based on integrated modeling, *Energy Conversion and Management* **135** (2017) 336, 350.
- [18] DUFFLE, J. A., BECKMAN, W. A., *Solar Engineering of Thermal Processes*, John Wiley and Sons, USA (2013).



- [19] SCHWARZBOZL, P., PITZ-PAAL, R., SCHMITZ, M., Visual HFLCAL-A Software Tool for Layout and Optimization of Heliostats Fields, Proceedings SolarPACES, Berlin (2009).
- [20] BESARATI, S. M., GOSWAMI, D. Y., STEFANAKOS, E. K., Optimal heliostat aiming strategy for uniform distribution of heat flux on the receiver of a solar power tower plant, *Energy Conversion and Management* **84** (2014) 234, 243.
- [21] WANG, K., HE, Y., CHENG, Z., A design method and numerical study for a new type parabolic trough solar collector with uniform solar flux distribution, *Science China Technological Sciences* **57** 3 (2014) 531, 540.
- [22] HE, Y. L., et al., Numerical simulation of solar radiation transmission process for the solar tower power plant: from the heliostat field to the pressurized volumetric receiver, *Applied Thermal Engineering* **61** 2 (2013) 583, 595.
- [23] WANG, K., HE, Y. L., QIU, Y., ZHANG, Y., A novel integrated simulation approach couples MCRT and Gebhart methods to simulate solar radiation transfer in a solar power tower system with a cavity receiver, *Renewable Energy* **89** (2016) 93, 107.
- [24] WAH, H., KYAING, N. S., Design Calculations of Heliostat Field Layout for Solar Thermal Power Generation, 105th The IIER International Conference, Bangkok, Thailand (2017).

## ANNEX I VAPOUR POWER CYCLE

The most efficient power cycle working between two specified temperatures is the Carnot cycle [I-1]. It is not the realistic and suitable power cycle for power generation, because of the several impracticalities such as the maximum temperature limit, high moisture content of the steam, and the compression of liquid-vapour mixture. These impracticalities can be eliminated by using the Rankine cycle, which is the ideal power generation cycle for power plants using water/vapours (both fossil fuel, and nuclear power based).

### I-1. IDEAL RANKINE CYCLE

The ideal Rankine cycle components and the associated temperature-entropy ( $T$ - $s$ ) diagram is shown in Fig. I-1 (a) and (b), respectively. It consists of four processes associated with four components. It does not consider any internal irreversibility as the heat transfer processes are assumed to be very slow. Water is used as the working fluid.

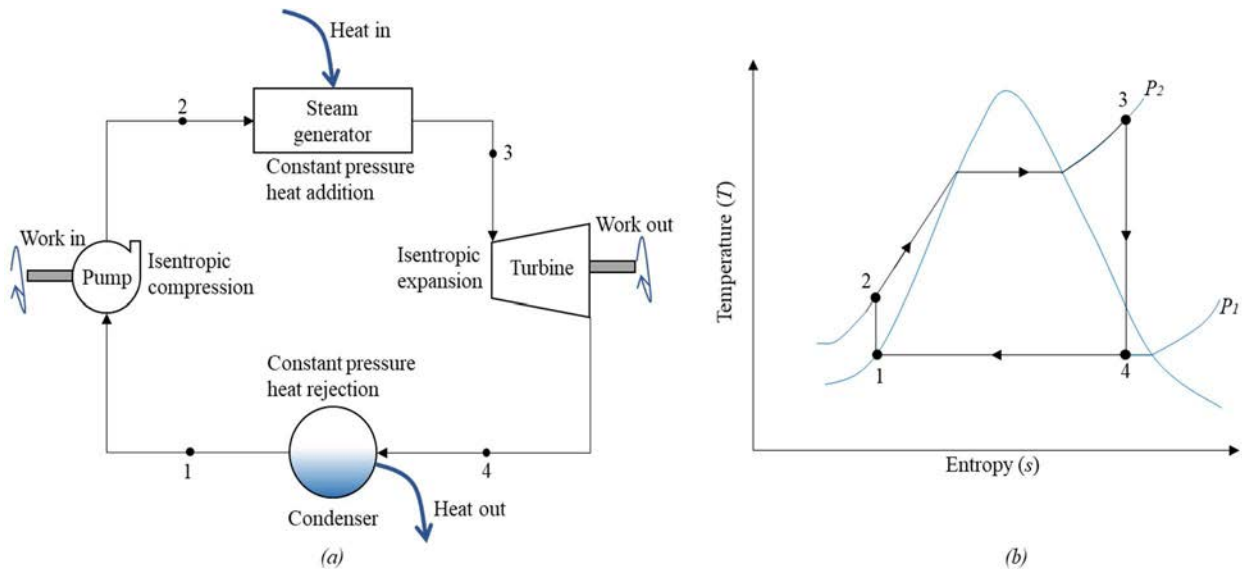


FIG. I-1. Ideal Rankine cycle: (a) components, (b)  $T$ - $s$  diagram.

Water enters the pump as saturated liquid (state 1) and is compressed isentropically from the condenser pressure ( $P_1$ ) to the steam generator pressure ( $P_2$ ). The compression (process 1-2) increases the water temperature by small differential as shown in Fig. I-1 (b). Due to increase in pressure, water as a subcooled liquid (state 2), enters the steam generator, where it is converted to superheated steam (state 3) following the constant pressure line  $P_2$  (process 2-3). The superheated steam then expands isentropically through the turbine blades and produce work by rotating the turbine shaft (process 3-4). The isentropic expansion reduces the pressure and temperature of the steam to condenser pressure and saturated temperature (state 4). The liquid-vapour mixture (state 4) transfers the heat to the heat sink through the condenser at the constant pressure (process 4-1), and saturated liquid is obtained at the exit of condenser (state 1). The area under the process curve 2-3 represents the amount of heat added to water, whereas the area under the process curve 4-1 represents the heat rejected in a condenser. The area enclosed by

these curves is the work out in the Rankine cycle. The efficiency of the ideal Rankine cycle is simply the ratio of work out to heat added [I-1].

The cycle efficiency can be increased by decreasing the condenser pressure, increasing the turbine inlet temperature, or increasing the steam generator pressure. Decreasing the condenser pressure increases the amount of heat required to achieve the state 3 in Fig. I-1 (b), but it also increases the work output from the turbine and the net effect is the higher efficiency. Increasing the turbine inlet temperature at constant pressure shifts the state 3 in Fig. I-1 (b) and increases the turbine output work and efficiency. Increasing the steam generator pressure increases the temperature at which heat is added, thus resulting in decreased input heat required to attain state 3 shown in Fig. I-1 (b), and increased efficiency.

## I-2. ACTUAL RANKINE CYCLE

The ideal Rankine cycle can only be obtained if there are no frictional losses and irreversibility associated with cycle components, which is not practical. The actual Rankine cycle is shown in Fig. I-2 in comparison with the ideal Rankine cycle [I-1]. It deviates from ideal Rankine cycle because of following:

- Pressure losses in steam generator (process 2-3), condenser (process 4-1) and the connecting components (pipes, valves, etc.);
- Heat loss in steam generator (process 2-3) and the connecting components;
- Irreversibility in pump (process 1-2) and turbine (process 3-1).

Pressure losses in the steam generator and the connecting pipes are compensated by pumping the fluid at higher pressure than required, which needs a relatively larger pump input power. Heat losses are compensated by transferring more heat to the fluid than it is required. However, the irreversibility in the pump and the turbine are dealt by introducing the isentropic efficiencies.

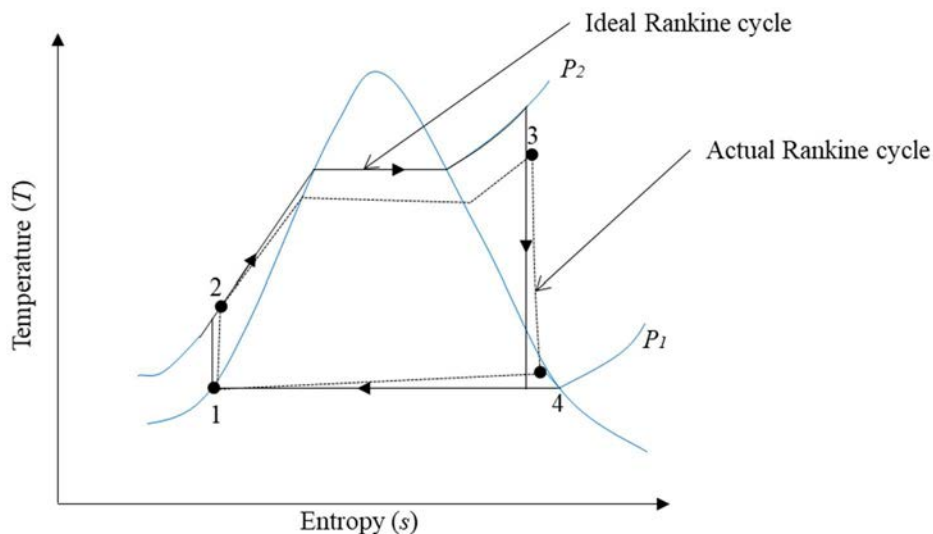


FIG. I-2. Comparison of actual Rankine cycle with ideal Rankine cycle (adopted from [I-1]).

### I-3. IDEAL REGENERATIVE RANKINE CYCLE

The analysis of the ideal Rankine cycle (Fig. I-1) reveals that the sensible part of the heat is supplied at low temperatures during the constant pressure heat addition (process 2-3), which decreases the average temperature at which heat is added to the Rankine cycle and decreases the efficiency. To increase the average temperature for heat addition feedwater heaters (open, close, or combined) are used by taking a portion of steam (called bleed steam) from turbines at various points. This results in increase in average temperature at which heat is added to the Rankine cycle and thus increases the cycle efficiency [I-2].

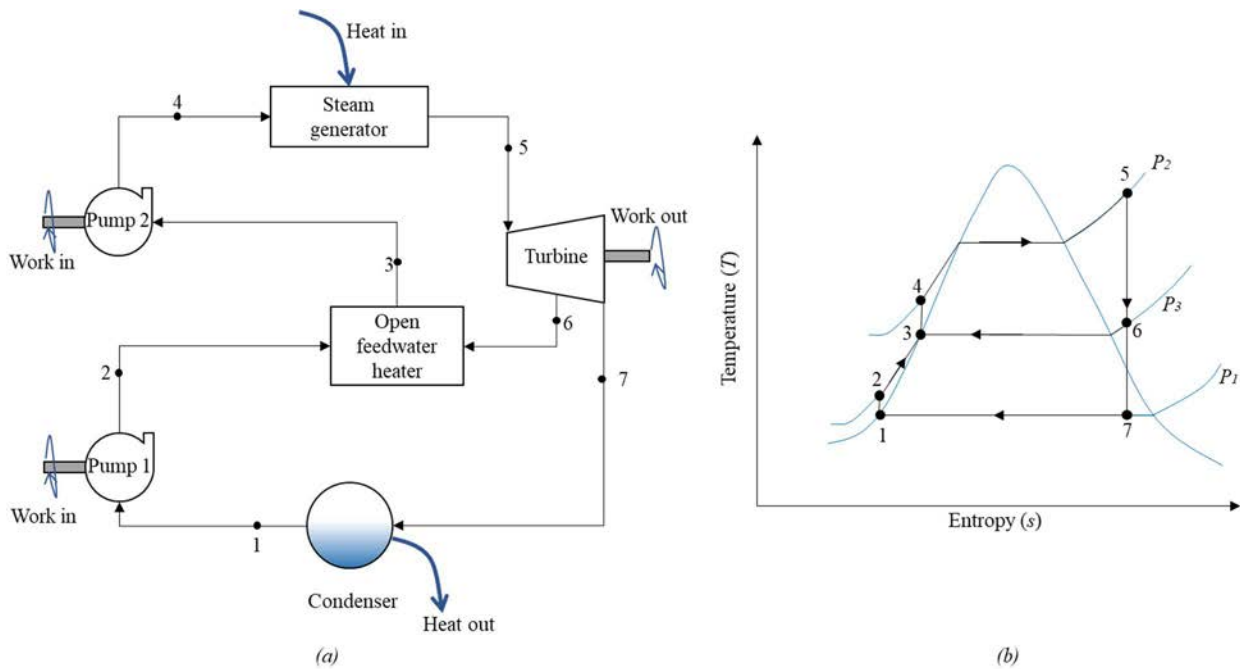


FIG. I-3. Ideal regenerative Rankine cycle: (a) components (adopted from [I-1]), (b)  $T$ - $s$  diagram (adopted from [I-1]).

Figure I-3 (a) and (b) represents the ideal regenerative Rankine cycle components and the associated  $T$ - $s$  diagram, respectively. The bleed steam at intermediate pressure ( $P_3$ ) is taken from the turbine at state 6 for providing the sensible heat during constant pressure heat addition process. The remaining steam continues to expand isentropically through the turbine (process 6-7); rejects heat through the condenser (process 7-1) and then pumped to the intermediate pressure by pump 1 (process 1-2). The subcooled water at state 2 and the bleed steam at state 6 mixed in open feed water heater to give saturated liquid at state 3. The saturated liquid is then pumped to state 4 before entering to the steam generator, which then heats the water to superheated steam. The portion of the heat (process 2-3) is supplied internally to the liquid, reducing the external heat addition to the Rankine cycle (process 4-5). This results in increased cycle efficiency [I-2].

In actual cycles combination of open and closed feedwater heaters are used for regenerative purpose to reduce the cycle irreversibility. The bleed steam from the turbine can also be used for cogeneration purpose which can increase the overall efficiency of the combined system.

#### I-4. RANKINE CYCLE IN PRESSURIZED WATER REACTORS

Figure I-4 shows a simplified Rankine cycle in pressurized water reactor. The schematic of complete system used in Rankine cycle is shown in Fig. I-4 (a). The reactor coolant pump and the pressurizer are not modelled, because pressure losses are neglected inside the reactor pressure vessel, steam generator and the connecting components. In the primary loop, water is heated from temperature  $T_b$  (state 'b') to  $T_a$  (state 'a') inside the reactor pressure vessel under constant pressure  $P_3$  as shown on  $T$ - $s$  diagram in Fig. I-4 (b). The water in primary loop then enters the steam generator and transfer the heat to the water in secondary side. In the primary side only the temperature of the water decreases (state 'a' to state 'b'), whereas in the secondary side the temperature as well as the phase of the water changes (subcooled water at state 2 to superheated steam at state 3 as shown in Fig. I-4 (c)). The superheated steam expands isentropically through the turbine producing the work, which then rejects heat through the condenser and converts to saturated liquid (state 1) and pumped again to the steam generator pressure (state 2).

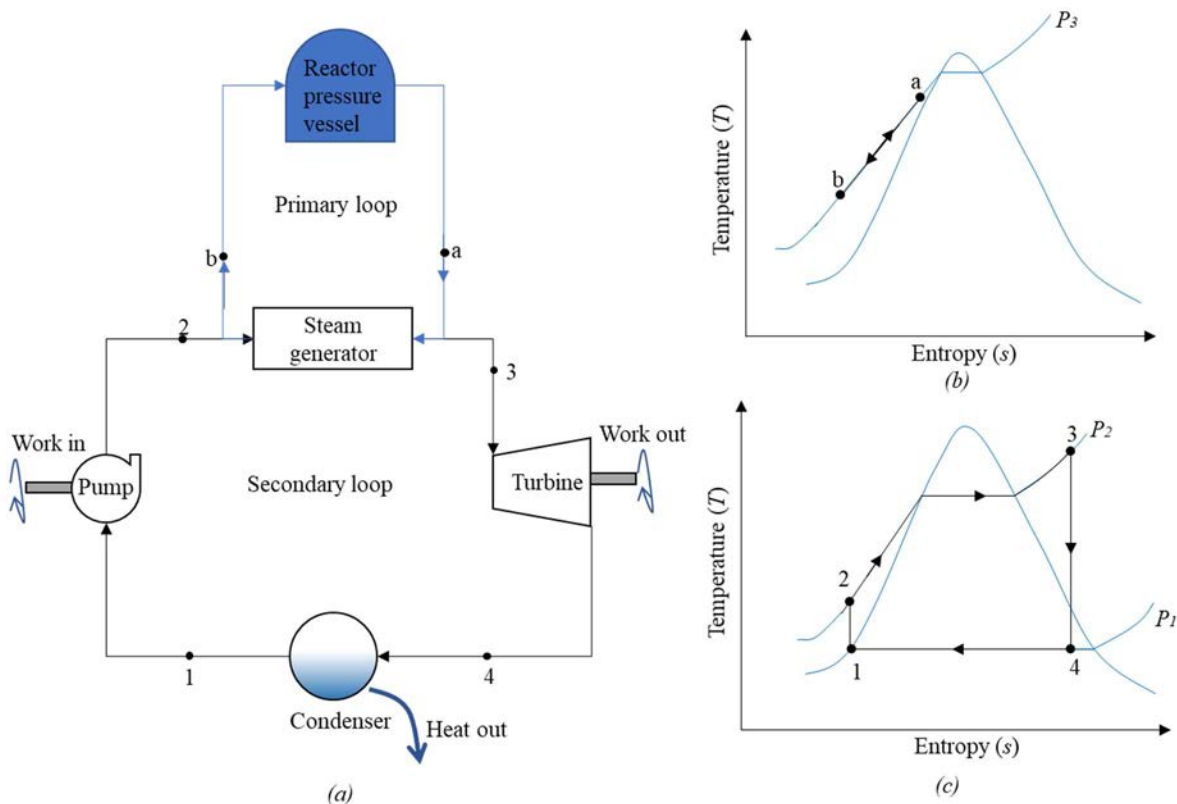


FIG. I-4. Rankine cycle in pressurized water reactors: (a) components, (b)  $T$ - $s$  diagram for primary side (adopted from [I-1]), (c)  $T$ - $s$  diagram for secondary side (adopted from [I-1]).

The  $T$ - $s$  diagrams for both the primary and secondary system is combined in a single  $T$ - $s$  diagram inside steam generator as shown in Fig. I-5. The temperature at state 'a' in the primary loop is higher than temperature at state '3' in the secondary loop. Similarly, the temperature at state 'b' in the primary loop is higher than the temperature at state '2' in the secondary loop. The minimum temperature difference (state 'c' in primary loop) occurs when the temperature in secondary loop reaches the saturation temperature and is called pinch point temperature

difference. It dictates the performance and irreversibility in steam generator [I-2]. A similar  $T-s$  diagram can also be drawn for the condenser in the Rankine cycle to show the irreversibility and the performance of the condenser.

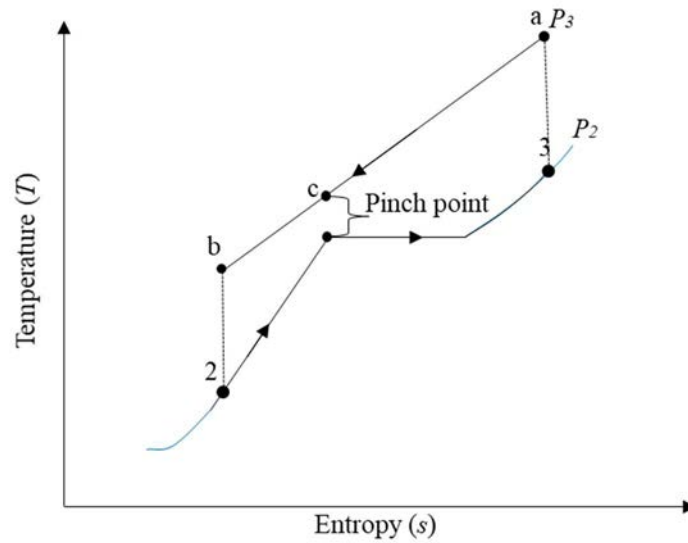


FIG. I-5.  $T-s$  diagram for the steam generator of pressurized water reactor (adopted from [I-1]).

#### REFERENCES TO ANNEX I

- [I-1] CENGEL, Y. A., BOLES, M. A., KANOGLU, M., Thermodynamics: An Engineering Approach, McGraw Hill, New York (2011).
- [I-2] SARKAR, D., Thermal Power Plant: Design and Operation, Elsevier, Amsterdam (2015).



## ANNEX II CONCENTRATED SOLAR POWER PLANTS

Concentrated solar power (CSP) technologies use reflectors to focus and concentrate the solar radiations onto a solar energy receiver, where the solar radiations are absorbed and converted into heat. Unlike photovoltaic cells which generates electricity, CSP produces heat which can be either used directly for industrial processes (hydrogen production, fertilizers etc.) or to produce the steam for generating electricity through turbine and generators [II-1]. CSP plants when integrated with energy storage devices become dispatchable potential application for electricity production [II-2].

Large number of reflecting mirrors with sun tracking controls are used to get highly concentrated solar radiations at the receiver. The higher concentrations lead to higher temperatures for steam generation and thus the better efficiency. However, a major technological challenge with CSP is to get the required optical precision and minimum environmental influence with lowest cost.

### II-1. TYPES OF CSP TECHNOLOGIES

In practice four different basic technologies are used for CSP plants that include parabolic trough reflectors, linear Fresnel reflectors, dish type reflectors and the solar power tower.

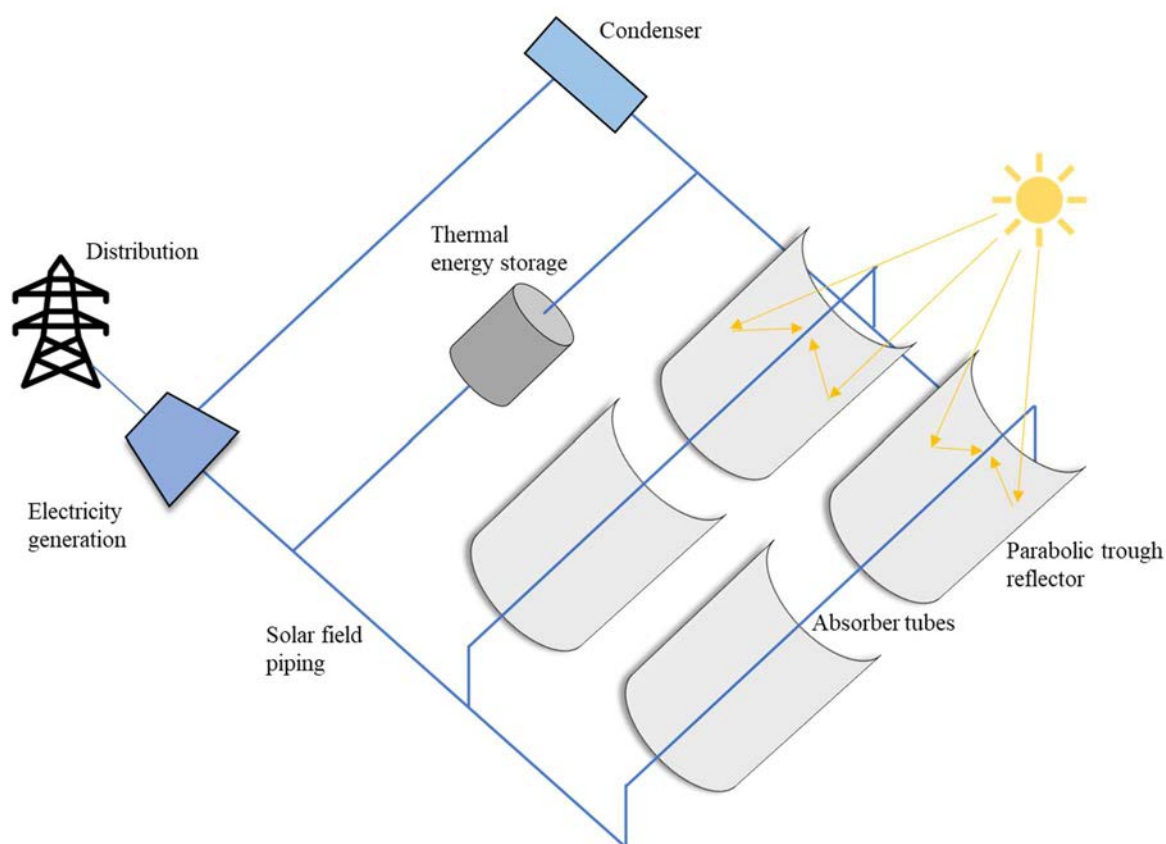


FIG. II-1. Parabolic trough reflector CSP plant.



Figure II–1 shows a schematic of the parabolic trough reflector CSP plant. In this type of CSP plant, parabolic mirrors are used to concentrate the solar radiations on an axial absorber tube passing through the focal point of each parabolic trough. The absorber tube is specially designed and contains a thermal fluid which allows heating up to 400°C. Solar field piping carries the heated thermal fluid to thermal energy storage, where the energy is stored and used for electricity generation. Uniaxial control is provided to the parabolic troughs for tracking the location of the sun [II–2].

Figure II–2 shows a schematic of linear Fresnel reflector CSP plant which is similar to the parabolic trough reflector. It consists of single centrally located fixed absorber tube, on which the solar radiations are concentrated through Fresnel reflectors.

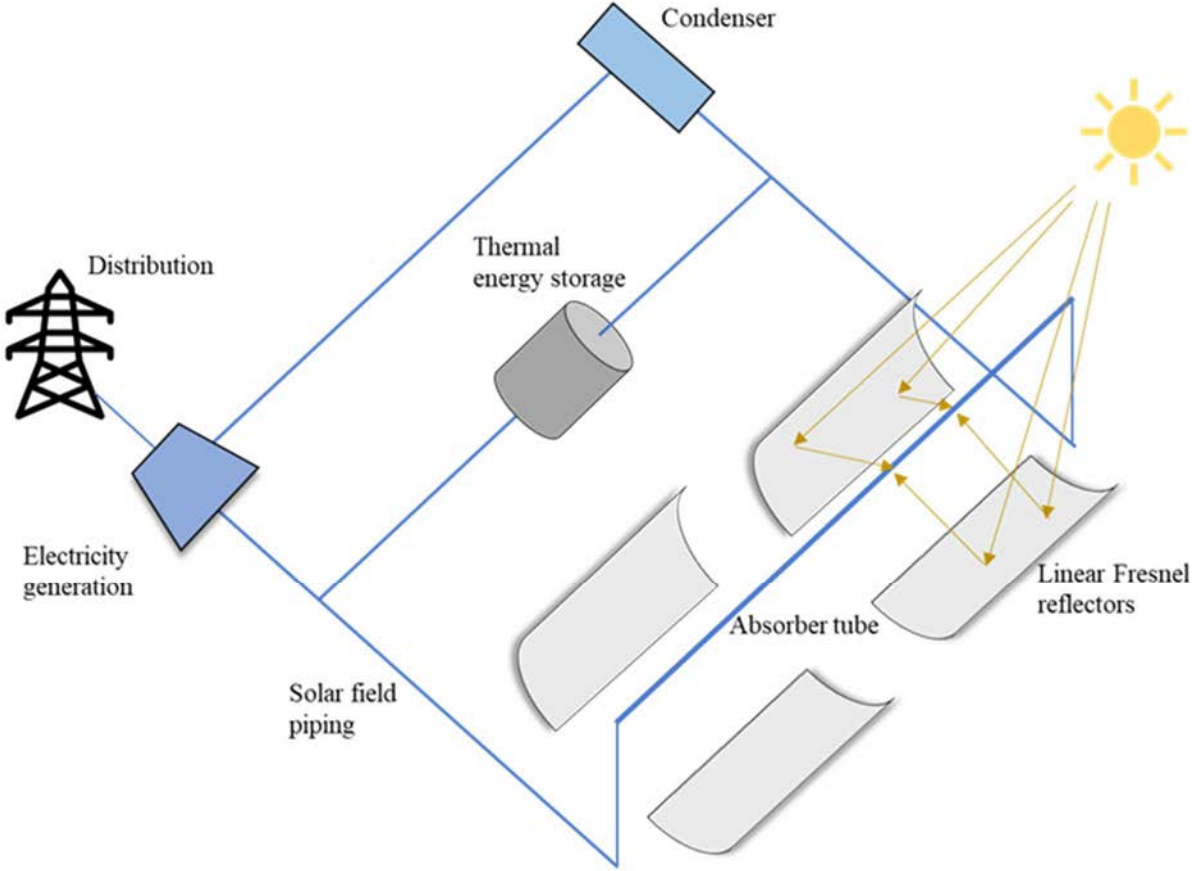


FIG. II–2. Linear Fresnel reflector CSP plant.

Figure II–3 shows a schematic of dish type reflector CSP plant. In this type of CSP plant several dish type concave mirrors are used to concentrate the solar radiation on small power conversion units. The power conversion units are located at the focal point of each dish and converts the directed solar thermal radiation directly into electrical power [II–1]. The electrical power is then distributed to the final users.

Figure II–4 shows a schematic of solar power tower CSP plant. In this type of CSP plant, biaxially controlled, thousands of heliostats are used to concentrate the solar radiations on centrally located solar power tower receiver. The energy from the concentrated solar radiations

can increase the increase the temperature at receiver beyond 1000°C. The heat is absorbed by the heat transfer medium in solar power tower, which transports the energy to the thermal storage in the range 300–700 °C depending on the type of heat transfer medium (water/steam or molten salt). The size of single heliostat can be as large as 200 m<sup>2</sup>, and it consists of large number of mirrors placed side by side on a single platform. The stored thermal energy is used for electricity production, which is then distributed to final users.

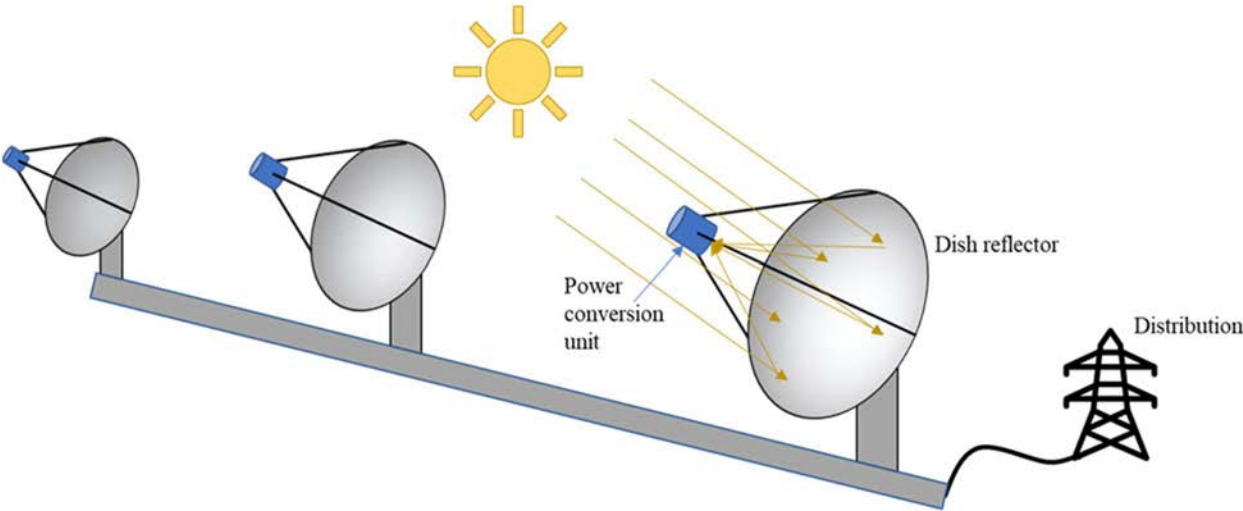


FIG. II-3. Dish type reflector CSP plant.

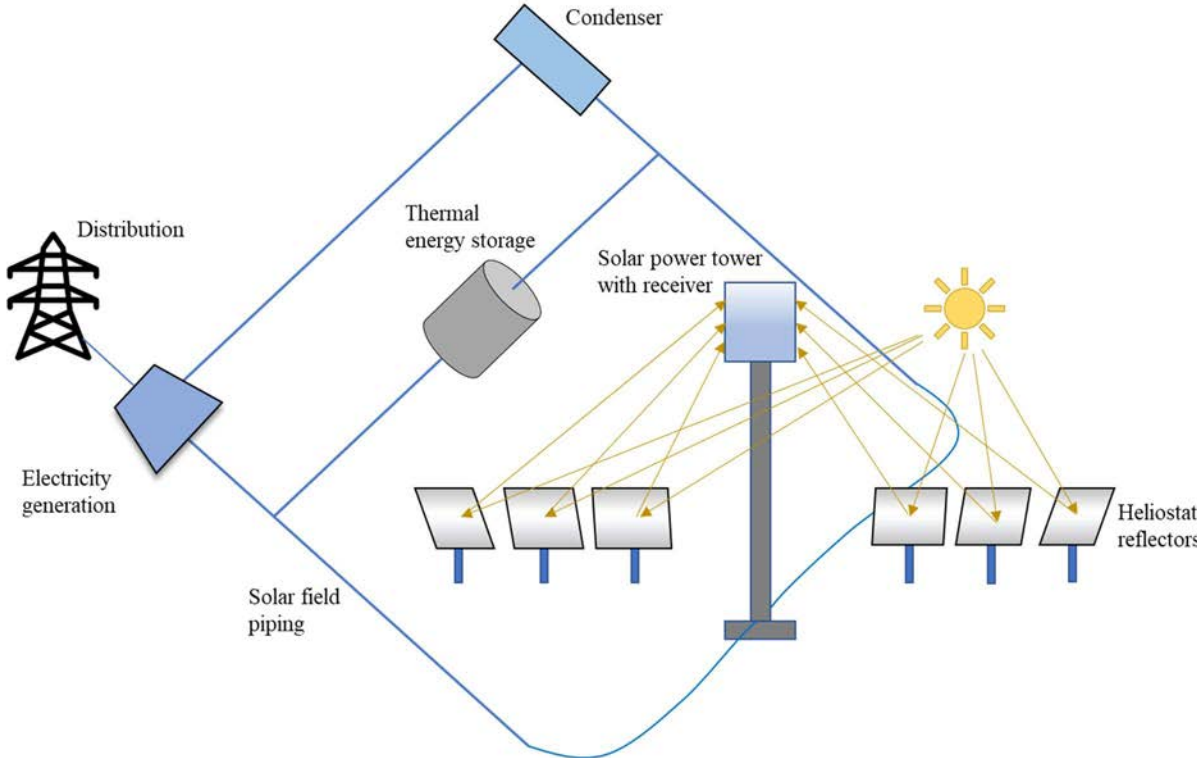


FIG. II-4. Solar tower CSP plant.

## II-2. ENVIRONMENTAL IMPACTS OF CSP PLANTS

Several factors need to be considered to analyse the environmental impact of CSP plants. The first one is the greenhouse gas emissions. The advent and integration of thermal storage systems with CSP plants results in increased availability without using fossil fuel power plants, thus resulting in decreased greenhouse gas emissions throughout the CSP plant life cycle. Almost all the greenhouse gas emissions in new CSP plants comes from the manufacturing of construction materials like glass, steel, concrete etc [II-1].

The second important factor is the land requirement which is about 0.01 km<sup>2</sup>/GWh per year for CSP plants [II-3]. Since they are primarily built in desert areas or on non-arable land; the land requirement is not an issue. However, there exists a risk to birds and insects' life. The studies have showed that appropriate control of mirrors can lower this risk [II-1].

Another important factor is the visual impact of CSP plants. The reflections from the heliostats and the strong brightness of the solar power tower can be disturbing to surrounding areas. However, the hazard values are much lower than one caused by sun itself. In summary, the overall environmental impact of CSP plants is very low as compared to the fossil fuel power plants.

## II-3. CSP PLANTS ACROSS THE WORLD

Global CSP generation capacity at the end of 2020 was 6.7 GW [II-4], from several CSP plants that are in operation across the world. Solar power and chemical energy systems (SolarPACES), an international program of the international energy agency have prepared a comprehensive data on CSP projects around the world that includes several technologies (parabolic trough, solar tower, linear-Fresnel, and dish type), which are either operational, under construction or under development [II-5]. Table II-1 shows the details of few CSP plants that are currently in operation. Analysis of database reveals that the parabolic trough based CSP plants are the most common across the world, followed by solar tower CSP plants, whereas none of the dish type CSP plant is operational yet.

TABLE II-1. OPERATIONAL CSP PLANTS ACROSS THE WORLD [II-5]

<b>Power station</b>	<b>Location</b>	<b>Technology Type</b>	<b>Nominal Capacity (MW)</b>	<b>Storage Capacity (hrs.)</b>
Noor III	Morocco	Solar power tower	150	7
Khi Solar One	South Africa	Solar power tower	50	2
Kathu Solar Park	South Africa	Parabolic trough	100	5
La Florida	Spain	Parabolic trough	50	7.5
Augustin Fresnel 1	France	Linear Fresnel	0.3	0.25

## REFERENCES TO ANNEX II

- [II-1] BENITEZ, D., et al., Solar Thermal Power Plants: Heat, Electricity and Fuels from Concentrated Solar Power, German Aerospace Center (DLR) Institute of Solar Research, Cologne (2021).

- [II-2] HELLER, P. (ed.), *The Performance of Concentrated Solar Power Systems: Analysis, Measurement and Assessment*, Woodhead Publishing, UK (2017).
- [II-3] ONG, S., et al., *Land-use Requirements for Solar Power Plants in the United States*, National Renewable Energy Lab (NREL), Rep. No. NREL/TP-6A20-56290, US (2013).
- [II-4] INTERNATIONAL ENERGY AGENCY, *Concentrated Solar Power (CSP)*, IEA, Paris (2021). <https://www.iea.org/reports/concentrated-solar-power-csp>
- [II-5] NATIONAL RENEWABLE ENERGY LABORATORY, *Solar Power and Chemical Energy Systems (Solar PACES)*, NREL, Concentrating Solar Power Projects. <https://solarpaces.nrel.gov/>



## ABBREVIATIONS

CSP	Concentrated Solar Power
HES	Hybrid Energy Systems
NPP	Nuclear Power Plant
SMR	Small Modular Reactor
T-s	Temperature-Entropy



## CONTRIBUTORS TO DRAFTING AND REVIEW

Ahmad, A.	Pakistan Institute of Engineering and Applied Sciences
Jevremovic, T.	International Atomic Energy Agency
Mubashir, W.	Pakistan Institute of Engineering and Applied Sciences
Rasheed, K.	Pakistan Institute of Engineering and Applied Sciences
Rehman, H ur.	International Atomic Energy Agency
Riaz, W.	International Atomic Energy Agency
Sungur, N.	International Atomic Energy Agency





## ORDERING LOCALLY

IAEA priced publications may be purchased from the sources listed below or from major local booksellers.

Orders for unpriced publications should be made directly to the IAEA. The contact details are given at the end of this list.

### NORTH AMERICA

***Bernan / Rowman & Littlefield***

15250 NBN Way, Blue Ridge Summit, PA 17214, USA

Telephone: +1 800 462 6420 • Fax: +1 800 338 4550

Email: [orders@rowman.com](mailto:orders@rowman.com) • Web site: [www.rowman.com/bernan](http://www.rowman.com/bernan)

### REST OF WORLD

Please contact your preferred local supplier, or our lead distributor:

***Eurospan Group***

Gray's Inn House  
127 Clerkenwell Road  
London EC1R 5DB  
United Kingdom

***Trade orders and enquiries:***

Telephone: +44 (0)176 760 4972 • Fax: +44 (0)176 760 1640

Email: [eurospan@turpin-distribution.com](mailto:eurospan@turpin-distribution.com)

***Individual orders:***

[www.eurospanbookstore.com/iaea](http://www.eurospanbookstore.com/iaea)

***For further information:***

Telephone: +44 (0)207 240 0856 • Fax: +44 (0)207 379 0609

Email: [info@eurospangroup.com](mailto:info@eurospangroup.com) • Web site: [www.eurospangroup.com](http://www.eurospangroup.com)

### Orders for both priced and unpriced publications may be addressed directly to:

Marketing and Sales Unit

International Atomic Energy Agency

Vienna International Centre, PO Box 100, 1400 Vienna, Austria

Telephone: +43 1 2600 22529 or 22530 • Fax: +43 1 26007 22529

Email: [sales.publications@iaea.org](mailto:sales.publications@iaea.org) • Web site: [www.iaea.org/publications](http://www.iaea.org/publications)



INTERNATIONAL ATOMIC ENERGY AGENCY  
VIENNA